Responses to comments from referee #2 on the paper "Reconstruction of super-resolution fields of ocean pCO_2 and air-sea fluxes of CO_2 from satellite imagery in the Southeastern Atlantic", *by I. Hernández-Carrasco et al.*

We are grateful to the reviewer for her/his comments that helped us to improve our manuscript. The original comments are shown in italics, and our detailed response can be found in normal typeface below every comment and the corresponding changes made in the revised manuscript.

Please note that we added two co-authors, with their approval, in our publication to be in agreement with the SOCAT atlas rules when using SOCAT in situ data. The two authors are:
M. Gonzalez-Davila and J. M. Santana-Casiano from the Instituto de Oceanografia y Cambio Global, Universidad de Las Palmas de Gran Canaria, 35017, Las Palmas de Gran Canaria, Spain.

Hernandez-Carrasco et al present an interesting new approach to map the partial pressure of CO2 in the surface ocean and the resulting air-sea gas flux, using satellite data. The authors convincingly show that their new high resolution approach obtains better results than a low resolution product (CARBONTRACKER) in the Benguela system when being compared to in-situ observations. The manuscript offers a method to the reader that on the one hand can be used to monitor the carbon cycle in the important EBUS regions but further has the potential to be applied globally.

I do believe the manuscript offers (a) a novel approach, (b) is clearly written – particularly the method section is easy to follow for the reader – and (c) describes an approach with potential for many future applications, hence I do recommend the manuscript for publication in BG. My specific comments below are intended to further improve the manuscript:

Response :
We thank the reviewer for his/her positive comments.

Specific comments:

General:

I only have one overarching point of criticism and this is the choice of data. While the authors do a great job testing several satellite chlorophyll-a and sea surface temperature products, the more fundamental question is why temperature and chlorophyll alone? E.G. it becomes very clear when looking at figure 11 (see longitudes 12.5 to 13.5 differences >20 µatm) that there is a stronger in-situ to product disagreement close to shore. Is this not a sign that near the coast the available data streams are possibly not enough to capture all the variability, whereas the more open ocean areas are better represented? At least some discussion would be useful.

Response: To address this comment we have plotted in Fig 1 (see below) (pCO_2^{insitu} vs. pCO_2^{ctrack}) and (pCO_2^{insitu} vs. pCO_2^{infer}) with points coloured by longitude using all the CarbonTracker and inferred pCO_2 values in the intersections with in-situ pCO2 during 2006 and 2008. This is for the case using Globcolour OC and OSTIA SST in the reconstruction of pCO2.
We have used this scatter plot to see the difference in the results between points close to the coast with those in the open ocean. For longitudes greater than 10 degrees (closer to the coast) pCO_2^{ctrack} and pCO_2^{infer} values are overestimated with more points closer to the diagonal for longitudes smaller than 10 degrees (open ocean region). This shows that near the coast the available input data do not capture all the variability, whereas the more open ocean areas are better represented.

This could be explained by the attenuation of the transitions fronts revealed by the merged Globcolour and OSTIA products used to alleviate cloudiness issues but we have obtained the same results (not shown) using the different merged and non merged products combinations. Thus, this disagreement with in situ data close to the coast can only be induced by the shortcomings of the CarbonTracker products in regions near the coast.

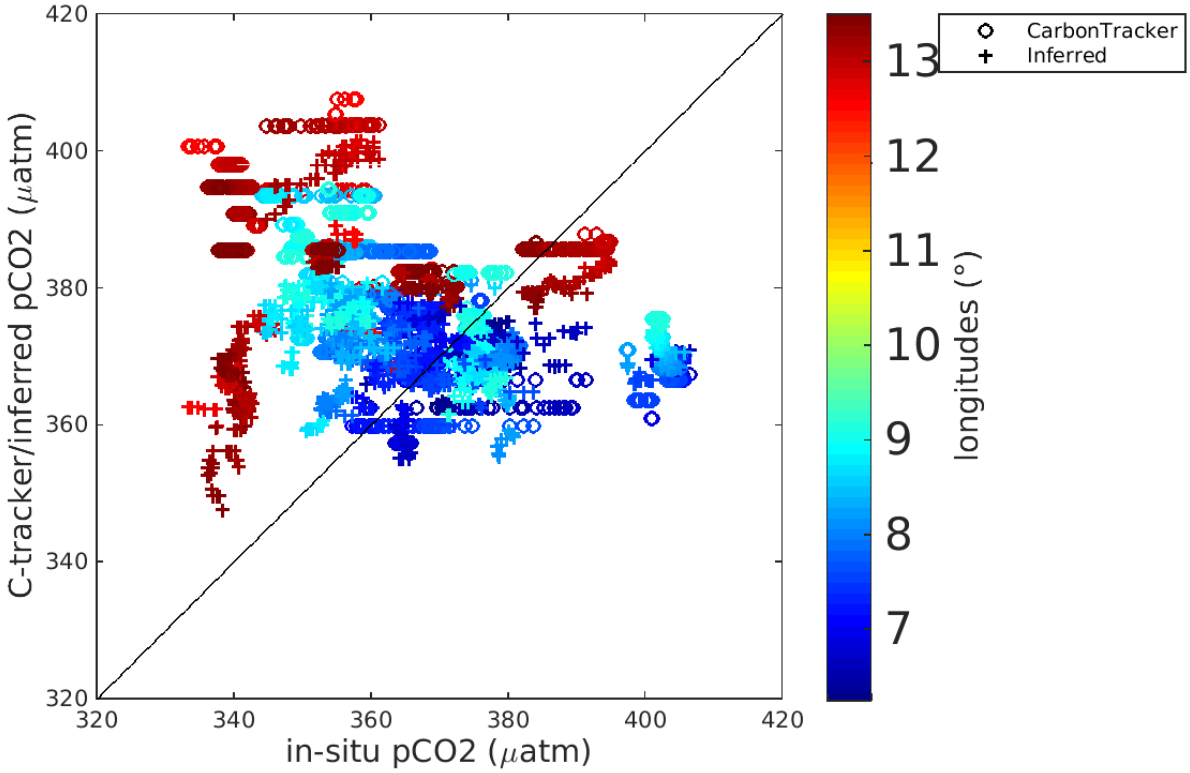

Fig 1. Scatter plot showing pCO2 values from CarbonTracker vs in-situ (in blue) and inferred vs in-situ (in red) at the intersections coloured as a function of longitude.

Abstract lines 1-4: circular sentence – remove or revise

Response : We rewrote these 3 lines as : "An accurate quantification of the role of the ocean as source/sink of Green House Gases (GHGs) requires to access the high-resolution of the GHG air-sea flux at the interface".

Introduction:

General: In the introduction there is a use of GHG's and CO2. The manuscript itself has its focus on CO2. Is the intention to motivate the reader that this approach can be used for all GHG's (then please state so explicitely)? Otherwise for clarity the use of GHG may be replaced by CO2

Response: This approach can be used to reconstruct all GHGs and we have included a sentence in the introduction to point out that the method has a wide applicability (Pag. 2 line 151-155). In

addition we have replaced GHG by CO2 in the cases where we focus, specifically, on CO2 (Page 2 lines 103 and 145).

page 1407 line 6: "resolve" not "solve"

Response: We have replaced "solve" by "resolve"

page 1407 line 8: "prevent us"

Response : It has been corrected.

page 1407 lines 19-20: Your products big advantage is its high resolution. It seems unfair in the introduction to present the 4x5 degree monthly climatology from Takahashi et al. as the most "advanced" pCO2 based product in this respect. There are high(er) temporal resolution products (Rödenbeck et al 2014 – 4x5 degree daily) and spatial resolution products (Nakaoka et al 2013 – 0.5x0.5 degree monthly; Landschützer et al 2014 - 1x1 degree monthly), which I think fir better in this discussion. This however does not change the message as the product presented in this study is still of higher resolution.

Response : Our intention in this discussion is not to present the product from Takahashi et al. as the most advanced but to enumerate current different approaches to estimate ocean pCO2 looking at their resolution. Thus, as suggested by the reviewer, we have included references on these products in lines 68-72 of the new manuscript to improve the discussion on different products at different spatial and temporal resolutions.

Page 1408 lines 10-11: I am not convinced that this statement is true for the ocean (at least not as much as it is for the land)

Response: We state that the spatial resolution of the CO2 fluxes in the ocean is not high enough from remote sensing data to resolve the small spatial variability of the source and sinks of CO2. On the other hand there is an uncertainty in extending ocean pCO2 over large gridded areas from limited coverage of the observations. Thus a better estimate of sub-gridscale processes and associated uncertainties using remote sensing is a high priority task to be conducted (Wang et al 2014, JGR).

Data:

page 1410 line 23: "ENVISAT" - throughout the manuscript, some abbreviations are explained (e.g. SCIAMACHY), whereas others (like e.g. ENVISAT) are not.

Response : We have explained the following abbreviations :

- ENVISAT (Environmental Satellite)
- LEGOS (Laboratoire d'Etudes en Géophysique et Océanographie Spatiales)
- SeaWiFS (Sea-Viewing Wide Field-of-View Sensor)
- JPL (Jet Propulsion Laboratory)
- PO.DAAC (Physical Oceanography Distributed Active Archive Center)

page 1411 lines 21-24: Globalview reports xCO2 in the atmosphere, whereas you report oceanic pCO2. Please clarify how you have dealt with this difference (unlike the fCO2 to pCO2 correction,

the xCO2 to pCO2 correction is not minor, hence it is not necessary neglectable when you compute air-sea fluxes, i.e. it has to be explicitly shown)

Response : We use the GLOBALVIEW time series to derive our atmospheric pCO2 value (and not the oceanic one).

Method:

page 1418 lines 13-17: Please consider splitting this sentence in two to make it easier to read.

Response : The sentence has been splitted in two as suggested by the reviewer (lines 494-499).

Results:

Although the merged products provide more coverage, the missing data from cloud coverage provide a major limitation to the product especially when air-sea fluxes of CO2 and their variability are investigated. This is a problem on the local, as well as on the global scale. In view of the future applications the authors mention, how do you plan to deal with this issue?

Response : Pottier et al. (2008) proposed a wavelet-based inference method for reconstructing ocean-color maps with missing pixels, so this methodology could be an avenue to follow to address the cloud coverage issue when the latter is not too severe.

Figures:

I was a bit puzzled looking at figure 1: Both products illustrate a strong carbon uptake along the coast (purple color) whereas I would have expected the opposite.

Response : Fig. 1 has been replotted with a different masking of the pixels (white instead of blue).

Figure 6d: Is this the average flux density (averaged by latitude)? I think the integrated flux (in GtC/s or TgC/yr, etc.) is a better visualization than the flux density and it additionally makes it easier to put the importance of the sink into a bigger (regional/global) perspective.

Response : In Fig 6d we have plotted a longitudinal transect of the maps shown in Figures 5e and 5f at a particular latitude (33.5°S in this case) in order to show the small scale spatial variability of the reconstructed pCO2 as compared to pCO2 derived from CarbonTracker.

Figures 7 and 8: Why is there a difference between the estimated area here and in figure 1?

Response : Fig. 1 has now the same area than the other figures.

References :

Wang, G., M. Dai, S. S. P. Shen, Y. Bai and Yi Xu (2014). Quantifying uncertainty sources in the gridded data of sea surface CO2 partial pressure. *J. Geophys. Res. Oceans*, **119**, 5181–5189, doi:10.1002/2013JC009577.

Manuscript prepared for Biogeosciences
with version 5.0 of the LaTeX class copernicus.cls.
Date: 23 April 2015

Reconstruction of super-resolution ocean pCO_2 and air-sea fluxes of CO_2 from satellite imagery in the Southeastern Atlantic

I. Hernández-Carrasco[1], J. Sudre[1], V. Garçon[1], H. Yahia[2], C. Garbe[3], A. Paulmier[1], B. Dewitte[1], S. Illig[1], I. Dadou[1], M. González-Dávila[4], and J. M. Santana-Casiano[4]

[1]LEGOS, Laboratoire d'Études en Géophysique et Océanographie Spatiales (CNES-CNRS-IRD-UPS), 31401 Toulouse, France
[2]INRIA, Institut National de Recherche en Informatique et en Automatique, Bordeaux, France
[3]IWR, Interdisciplinary Center for Scientific Computing, University of Heidelberg, Heidelberg, Germany
[4]Instituto de Oceanografía y Cambio Global, Universidad de Las Palmas de Gran Canaria, 35017, Las Palmas de Gran Canaria, Spain

Correspondence to: I. Hernández-Carrasco
(ismael.hernandez@legos.obs-mip.fr)

Abstract. An accurate quantification of the role of the ocean as source/sink of Green House Gases (GHGs) requires to access the high-resolution of the GHG air-sea flux at the interface. In this paper we present a novel method to reconstruct maps of surface ocean partial pressure of CO_2, pCO_2, and air-sea CO_2 fluxes at super resolution (4 km) using Sea Surface Temperature (SST) and Ocean Colour (OC) data at this resolution, and CarbonTracker CO_2 fluxes data at low resolution (110 km). Inference of super-resolution of pCO_2, and air-sea CO_2 fluxes is performed using novel nonlinear signal processing methodologies that prove efficient in the context of oceanography. The theoretical background comes from the Microcanonical Multifractal Formalism which unlocks the geometrical determination of cascading properties of physical intensive variables. As a consequence, a multiresolution analysis performed on the signal of the so-called singularity exponents allows the correct and near optimal cross-scale inference of GHGs fluxes, as the inference suits the geometric realization of the cascade. We apply such a methodology to the study offshore of the Benguela area. The inferred representation of oceanic partial pressure of CO_2 improves and enhances the description provided by CarbonTracker, capturing the small scale variability. We examine different combinations of Ocean Colour and Sea Surface Temperature products in order to increase the number of valid points and the quality of the inferred pCO_2 field. The methodology is validated using in-situ measurements by means of statistical errors. We obtain that mean absolute and relative errors in the inferred values of pCO_2 with respect to in-situ measurements are smaller than for CarbonTracker.

1 Introduction

The ocean can be thought of as a complex system in which a large number of different processes (e.g. physical, chemical, biological, atmosphere-ocean interactions) interact with each other at different spatial and temporal scales (Rind, 1999). These scales extend from millimeters to thousands of kilometers and from seconds to centuries (Dickey, 2003). In particular, recently there is a growing body of evidence that the upper few hundred meters of the oceans are dominated by submesoscale activity, covering the range 1-10 km, and that this activity is important to understand global ocean properties (Klein and Lapeyre, 2009). Accurately estimating the sources and sinks of GHGs at the air-sea interface requires to resolve these small scales (Mahadevan et al., 2004). However, the scarcity of oceanographic cruises and the lack of available satellite products for GHG concentrations at high resolution prevent us from obtaining a global assessment of their spatial variability at small scales. For example, from the in-situ ocean measurements the uncertainty of the net global ocean-atmosphere CO_2 fluxes is between 20 and 30% (IOCCP, 2007), and could be higher in the Oxygen Minimum Zones (OMZ) of the Eastern Boundary Upwelling Systems (EBUS) due to the extreme regional variability in these areas (Paulmier et al., 2008; Franco et al., 2014). This indeed suggests the design of proper methodologies to infer the fluxes

at high resolution from presently available satellite images data, in order to improve current estimates of gas exchanges between the ocean and the atmosphere.

The most commonly used methods to estimate air-sea CO_2 fluxes are based either on statistical methods, inverse modeling with atmospheric transport models or global coupled physical-biogeochemical models. Among others we can find the work by Takahashi et al. (2002, 2009) where they interpolate sea surface pCO_2 measurements with advanced statistical methods to provide climatological monthly maps of air-sea fluxes of CO_2 in the global surface waters at a spatial resolution of $4^\circ \times 5^\circ$. Global maps at the same spatial resolution but at higher temporal resolution (daily) have been estimated by Rödenbeck et al. (2014) by fitting the mixed-layer carbon budget equation to ocean pCO_2 observations. Beside the Takahashi's works an international effort to compile global surface CO_2 fugacity (fCO_2) measurements has been recently performed and reported in Pfeil et al. (2013); Bakker et al. (2014), and later interpolated by Sabine et al. (2013) generating a monthly gridded product with fCO_2 values in a 1°x1° grid cell. Other statistical approach based on the neural-network statistical method has been shown to be useful to estimate climatological and monthly 1°x1° maps of pCO_2 by Landschützer et al. (2014) and Telszewski et al. (2009) respectively. Gruber et al. (2009) used an inverse modeling of sources and sinks from the network of atmospheric CO_2 concentrations jointly with transport models. The third type of methods is based on the direct computations of the air-sea CO_2 fluxes in coupled physical-biogeochemical models incorporating the biogeochemical processes of the carbon dioxide system. In the latter, simulated surface ocean pCO_2 can be constrained with available ship observations as shown by Valsala and Maksyutov (2010).

Another new avenue to infer air-sea GHG fluxes is through inverse modeling applied to vertical column densities (VCD) extracted from satellite spectrometers, i.e. Greenhouse gases Observing SATellite (GOSAT) and SCanning Imaging Absorption SpectroMeter for Atmospheric CHartographY (SCIAMACHY), at low spatial resolution (Garbe and Vihharev, 2012). A global estimation of CO_2 fluxes in the ocean has been derived at $1^\circ \times 1^\circ$ of spatial resolution from global atmosphere observations used into a data assimilation system for CO_2 called CarbonTracker (Peters et al., 2007). In all these datasets the rather coarse spatial resolution leads to uncertainties in the actual estimate of the sources and sinks of CO_2, calling for an improvement of the resolution of CO_2 flux estimates.

In this regard, the last few years have seen the appearance of interesting new developments on multiscale processing techniques for complex signals coming from Earth Observations (Yahia et al., 2010). These methods make use of phenomenological descriptions of Fully Developed Turbulence (FDT) in nonlinear physics, motivated by the values taken on by Reynolds number in ocean dynamics. As predicted from the theory and also observed in the ocean, in a turbulent flow the coherent vortices (eddies) interact with each other stretching and folding the flow generating smaller eddies or small scale filaments and transition fronts characterized by strong tracer gradients (Frisch, 1995). This results in a cascade of energy from large to smaller scales. Therefore the inherent cascade of tracer variance under the turbulent flow dominates the variability of the geometrical distribution of tracers such as temperature or dissolved inorganic carbon, as shown by Abraham et al. (2000), Abraham and Bowen (2002), Turiel et al. (2005). Geometrical organization of the flow linked to the energy cascade allows to study its properties from the geometrical properties of any tracer for which the advection is the dominant process. The relationships between the cascade and the multifractal organization of FDT has been set up either in a canonical (Arneodo et al., 1995; Frisch, 1995) or microcanonical (Turiel et al., 2005; Bouchet and Venaille, 2012) descriptions. Within the microcanonical framework (MMF) the singularity exponents unlock the geometrical realization of the multifractal hierarchy. Setting up a multiresolution analysis on the singularity exponents computed in the microcanonical framework allows near optimal cross scale inference of physical variables (Sudre et al., 2015).

These advances open a wide field of theoretical and experimental research and their use in the analysis of complex data coming from satellite imagery has been proven innovative and efficient, showing a particular ability to perform fusion of satellite data acquired at different spatial resolutions (Pottier et al., 2008) or to reconstruct from satellite data currents maps at submesoscale resolution (Sudre et al., 2015). In this paper we apply these novel techniques emerging from nonlinear physics and nonlinear signal processing for inferring submesoscale resolution maps of the air-sea CO_2 fluxes and associated sinks and sources from available remotely sensed data. We use this methodology to derive cross scale inference according to the effective cascade description of an intensive variable, through a fusion process between appropriate physical variables which account for the fluxes exchanges between the ocean and the atmosphere. This approach is not only very novel in signal processing, but also connects the statistical description of acquired data with their physical content. This makes the approach useful to reconstruct all GHGs.

Unlike the Lagrangian approach to reconstruct tracer maps at high resolution (Berti and Lapeyre, 2014), our methodology works in the Eulerian framework and we do not need to know the trajectories of oceanic tracer particles but only high resolution instantaneous maps of tracers which can be directly obtained from remote sensing.

The Eastern Boundary Upwelling Systems (EBUS) and Oxygen Minimum Zones (OMZs) are likely to contribute significantly to the gas exchange between the ocean and the atmosphere (Hales et al., 2005; Waldron et al., 2009; Paulmier et al., 2011). The Benguela upwelling system, the region of interest in this study, is one of the highest produc-

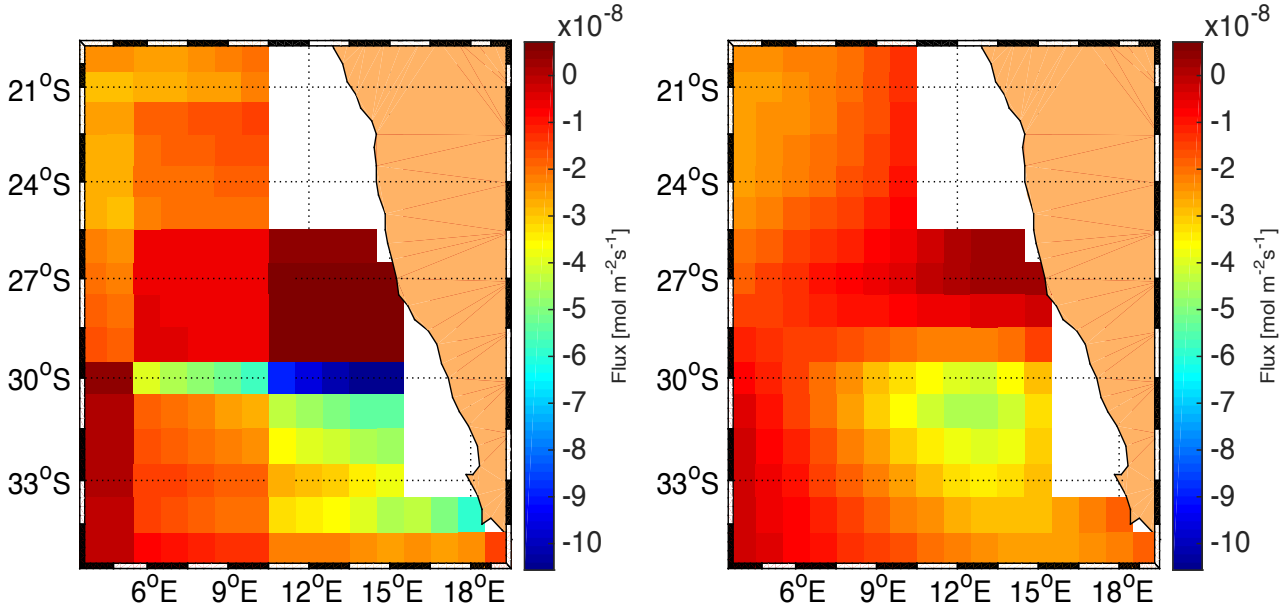

Fig. 1. Estimated fluxes from CarbonTracker data. Shown are the results on the Benguela upwelling system on March 23, 2006. Left are the CarbonTracker fluxes, right are our results.

tivity areas in the world ocean and may contribute significantly to the global air-sea CO_2 flux. More precisely, some studies using data from in-situ samples have found the region of Benguela to be an annual sink of CO_2 with -1.70 (in 1995 and 1996) and -2.02Mt C/year in 2005 (Santana-Casiano et al., 2009; Monteiro, 2010), with a strong variability between 2005 and 2006 from -1.17 to -3.24 mol C/m^2 per year, respectively (González-Dávila et al., 2009).

The paper is organized as follows: Sect. 2 describes the datasets used as input in our algorithm. Sect. 3 is devoted to describe the methodology used through the study. Statistical description of the input datasets is presented in Sect. 4. Results of the inference method are given in Sect. 5 by providing outputs of our algorithm, then evaluating the various satellite products and assessing the performance of the method using in situ measurements.

2 Data

The input data combines air-sea CO_2 fluxes at low resolution and satellite ocean data at high resolution. To validate the method we use in-situ measurements of oceanic pCO_2.

2.1 Input data: Air-sea CO_2 fluxes at low resolution

It is known that the evolution of a concentration, c, in the atmosphere is given by the advection-reaction-diffusion equation:

$$\frac{\partial c}{\partial t} = -u\nabla c + \frac{1}{\rho}\nabla(\rho T_d \nabla c) + \frac{1}{\rho}g + F, \quad (1)$$

with the wind field u, the density of the air ρ, the turbulent diffusivity tensor T_d, the chemical reaction rate g and the net flux at the air-sea interface F (Garbe et al., 2007, 2014). Using optimal control and inverse problem modeling, a map of F can be derived using Earth Observation data (Garbe and Vihharev, 2012). It would be ideal if we could use data of atmospheric CO_2 concentrations from space measured by satellite sensors such as SCIAMACHY (SCanning Imaging Absorption SpectroMeter for Atmospheric CHartographY) aboard ENVISAT (Environmental Satellite), in orbit since 2002, and GOSAT (Greenhouse gases Observing SATellite), in orbit since January 2009, to derive the air-sea flux. However SCIAMACHY and GOSAT sampling is not dense enough with very suboptimal sampling of the Benguela upwelling system. This led us to use data of CO_2 fluxes from CarbonTracker (http://www.esrl.noaa.gov/gmd/ccgg/carbontracker/) at spatial resolution of 1° x 1° (∼100 km x ∼100 km) (Peters et al., 2007). CarbonTracker system assimilates and integrates a diversity of atmospheric CO_2 data into a computation of surface CO_2 fluxes, using a state-of-the-art atmospheric transport model and an ensemble Kalman filter.

We obtain the partial pressure of ocean CO_2 by using the equation of the net flux in the air-sea interface:

$$F = \alpha K(p^{air}_{CO_2} - p^{ocean}_{CO_2}), \quad (2)$$

where α is the gas solubility, which depends on SST and Sea Surface Salinity SSS, and K, the gas transfer velocity, is a function of wind, salinity, temperature, sea state, which can be obtained from satellite data. To estimate the gas transfer velocity we use the well accepted relationships for the transfer velocity in air-sea gas exchange from wind speed, the parametrization developed by Sweeney et al. (2007). The CO_2 gas solubility is derived according to Weiss (1974). Input data for SST are derived from OSTIA (Operational SST and Sea Ice Analysis system) product, SSS are derived from LEGOS (Laboratoire d'Etudes en Géophysique et Océanographie Spatiales) product compiled by Delcroix et al. (2011) and winds from Cross Calibrated Multi-Platform Ocean surface winds from JPL (Jet Propulsion Laboratory) PO.DAAC (Physical Oceanography Distributed Active Archive Center, http://podaac.jpl.nasa.gov/). We assume a $p^{air}_{CO_2}$ to be constant in the domain of study and it is derived from the Globalview-CO2 product of the Cooperative Atmospheric Data Integration Project coordinated by Carbon Cycle Greenhouse Gases Group (GLOBALVIEW, 2013) (www.esrl.noaa.gov/gmd/ccgg/globalview/). We use values taken at the closest station off Benguela and closest to sea level, located at Ascension Island (7.97°S and 14.40°W) as our reference atmospheric CO_2.

The raw data of CarbonTracker fluxes of CO_2 in the area of interest are strongly binned and exhibit strong gradients across those bins. This turns out to be suboptimal for our super-resolution approach. Garbe and Vihharev (2012) have developed an optimal control approach to invert interfacial fluxes using a simplified inverse problem of atmospheric transport. The inverse problem is solved using the Galerkin finite element method and the Dual Weighted Residual (DWR) method for goal-oriented mesh optimization. An adaptation of this approach has been applied to the CarbonTracker data set. However, the estimations are expensive and computing results for all the time frames of interest was infeasible. Therefore, an anisotropic diffusion-based approach has been applied to the raw fluxes of the CarbonTracker data set. The diffusion is steered by the direction of the low-altitude wind field. The results thus retain the structure of the CarbonTracker fluxes very well while suppressing artifacts. Results are comparable to the physically more accurate approach of Garbe and Vihharev (2012). Examples of this process are shown in Fig. 1.

2.2 Input data: Satellite Ocean data at high resolution

Oceanic pCO_2 is a complex signal depending, at any spatial resolution, on sea surface temperature, salinity, chlorophyll concentration, dissolved inorganic carbon, alkalinity and nutrients concentrations. Both the biological pump, with chlorophyll a as a proxy, and the physical pump, driven by the temperature and salinity (e.g. solubility, water mass), govern the evolution of pCO_2, when dealing with CO_2 for instance, in the surface ocean.

We use here the high resolution satellite ocean data for chlorophyll a, as a proxy for the biological carbon pump and for Sea Surface Temperature (SST), as a proxy for the thermodynamical pump, (see Section 3.2 for more details on the connection of these oceanic variables).

2.2.1 Chlorophyll-a (Chl-a) from Ocean Colour (OC)

In this study we use Chl-a concentrations from two different Ocean Colour products: MERIS and GLOBCOLOUR. MERIS (MEdium Resolution Imaging Spectrometer Instrument) is on board the ENVISAT satellite and provides daily maps of ocean colour at 1/24° (∼4 km). Ocean colour from GLOBCOLOUR product is obtained by merging data provided by MODIS (MODerate Resolution Imaging Spectroradiometer), MERIS and SeaWiFS instruments. The Chl-a concentration is provided daily and at the spatial resolution equal to 1/24° (∼4 km). Ocean Colour data have been regridded at 1/32° by linear interpolation. GLOBCOLOUR products are generated using different merging methods (see the GLOBCOLOUR Product User Guide document in $http://www.globcolour.info/CDR\_Docs/GlobCOLOUR\_PUG.pdf$):

- **Averaging from single-instrument chl-a concentration**. In this case CHL1 daily level 3 (L3) products are generated for each instrument using the corresponding L2 data. At the beginning of the averaging process, an inter-calibration correction is applied to the MODIS and SeaWiFS (Sea-Viewing Wide Field-of-View Sensor) CHL1 daily L3 products in order to get compatible concentrations with respect to the MERIS sensor. The merged CHL1 concentration is then computed as the average of the MERIS, MODIS and SeaWiFS quantities, both as: an **arithmetic mean** or a **weighted average value (AVW)**. In the AVW method, values of CHL1 are weighted by the relative error for each sensor on the results of the simple averaging.

- **Garver-Siegel-Maritorena model (GSM)**. In this method single-instrument daily L3 fully normalized water leaving radiances (individually computed for each band) and their associated error bars are used by the GSM model. These radiances are not inter-calibrated before incorporation in the model (see Maritorena and Siegel (2005) for more details).

Snapshots of both Chl-a fields derived from MERIS and GSM GLOBCOLOUR corresponding to September 21, 2006 are displayed in Fig. 2 a) and b), respectively. This example shows the clear difference in the remote sensing coverage between the two products. The merged GLOBCOLOUR product yields a more covered Chl field than the one obtained

from MERIS. The merging algorithm in GLOBCOLOUR product tends to decrease the missing points induced by clouds for each individual instrument.

2.2.2 Sea Surface Temperature (SST)

We use SST derived from OSTIA and MODIS products. OSTIA (Operational SST and Sea Ice Analysis system) is a new analysis of SST that uses satellite data provided by the GHRSST (Group for High Resolution SST) project, together with in situ observations to determine the SST with a global coverage and without missing data. The datasets are produced daily and at spatial resolution of 1/20° (∼6km) performing a multi-scale optimal interpolation using correlation length scales from 10 km to 100 km (more details in Donlon et al. (2012)). The other SST product used in this study is derived from MODIS (MODerate Resolution Imaging Spectroradiometer) sensors carried on board the Aqua satellite since December 2002. This SST product is derived from the MODIS mid-infrared (IR) and thermal IR channels and is available in various spatial and temporal resolutions. We use Level-3 daily maps of SST at the spatial resolution of 1/24° (∼4 km) (Savtchenko et al., 2004). In Fig. 3 a) and b), we show one snapshot of SST from OSTIA and MODIS respectively corresponding to the same day on September 21, 2006. In the case of OSTIA products, the SST field is fully covered of points while for MODIS products there are gaps due to cloudiness. On other hand, MODIS product offers a more detailed visualization of the small structures. All SST data have been regridded at 1/32° by bilinear interpolation.

2.3 Validation data: in-situ measurements

Among the available data in SOCAT version 2 (Bakker et al., 2014) (Surface Ocean CO_2 Atlas, http://www.socat.info) over the 2000-2010 period in our region of interest we find the following cruises with pCO_2 measurements:

- **2000**, one cruise: *ANT-18-1*
- **2004**, one cruise: *0404SFC-PRT*
- **2005**, five cruises: *QUIMA2005-0804, QUIMA2005-0821, QUIMA2005-0922, QUIMA2005-1202, QUIMA2005-1220*
- **2006**, nine cruises: *GALATHEA, QUIMA2006-0326, QUIMA2006-0426, QUIMA2006-0514, QUIMA2006-0803, QUIMA2006-0821, QUIMA2006-0921, QUIMA2006-1013, QUIMA2006-1124*
- **2008**, seven VOS cruises: *QUIMA2008-1, QUIMA2008-2, QUIMA2008-3, QUIMA2008-4, QUIMA2008-5, QUIMA2008-6, QUIMA2008-7*
- **2010**, one cruise: *ANT27-1*

The small number of cruises found in one decade (24 cruises) shows that the scarcity of cruises in the Benguela region is a fact. This indeed demonstrates the crucial need of developing a robust method to infer high resolution pCO_2 from space. Moreover for some of these cruises, for instance, the track of GALATHEA cruise is too close to the coast and is out of the original CarbonTracker domain. Due to this restriction we only document the offshore conditions of this upwelling system. Owing to the relatively large number of cruises during 2005, 2006 and 2008 (a total of 20 cruises, representing 83% of all available cruise data from 2000 through 2010), in this validation, we focus the analysis on the set of QUIMA-cruises during 2005 (QUIMA2005), 2006 (QUIMA2006) and 2008 (QUIMA2008) and we present the global analysis using all available cruises during these three years. Santana-Casiano et al. (2009) analyzed this data to study the sea surface pCO_2, fCO_2 and CO_2 air-sea fluxes offshore of the Benguela upwelling system between 2005 and 2006 (for each month from July 2005 up to November 2006) and González-Dávila et al. (2009) extended the study including cruises data from 2007 to 2008. The QUIMA line crosses the region between 5°S and 35°S, with all the cruises following the same track.

3 Method

The idea behind the methodology hinges on the fundamental discovery of a simple functional dependency between the transitions - those being measured by the dimensionless values of the singularity exponents computed within the framework of the Microcanonical Multifractal Formalism - of the respective physical variables under study : SST, Ocean Colour and oceanic partial pressure (pCO_2). That functional dependency being adequately fitted into a linear regression model, it becomes possible to compute, at any given time, a precise evaluation of pCO_2 singularity exponents using SST, Ocean Colour and low resolution acquired pCO_2. Once these singularity exponents are computed, they generate a multiresolution analysis from which low resolution pCO_2 can be cross-scale inferred to generate a high resolution pCO_2 product.

3.1 Singularity exponents and the multifractal hierarchy of turbulence

In the ocean, the turbulence causes the formation of unsteady eddies on many scales which interact with each other (Frisch, 1995). Most of the kinetic energy of the turbulent motion is contained in the large scale structures. The energy cascades from the large scale structures to smaller scale structures by an inertial and essentially inviscid mechanism. This process continues, creating smaller and smaller structures which produces a hierarchy of eddies. Moreover, the ocean is a system displaying scale invariant behavior, that is, the correlations of

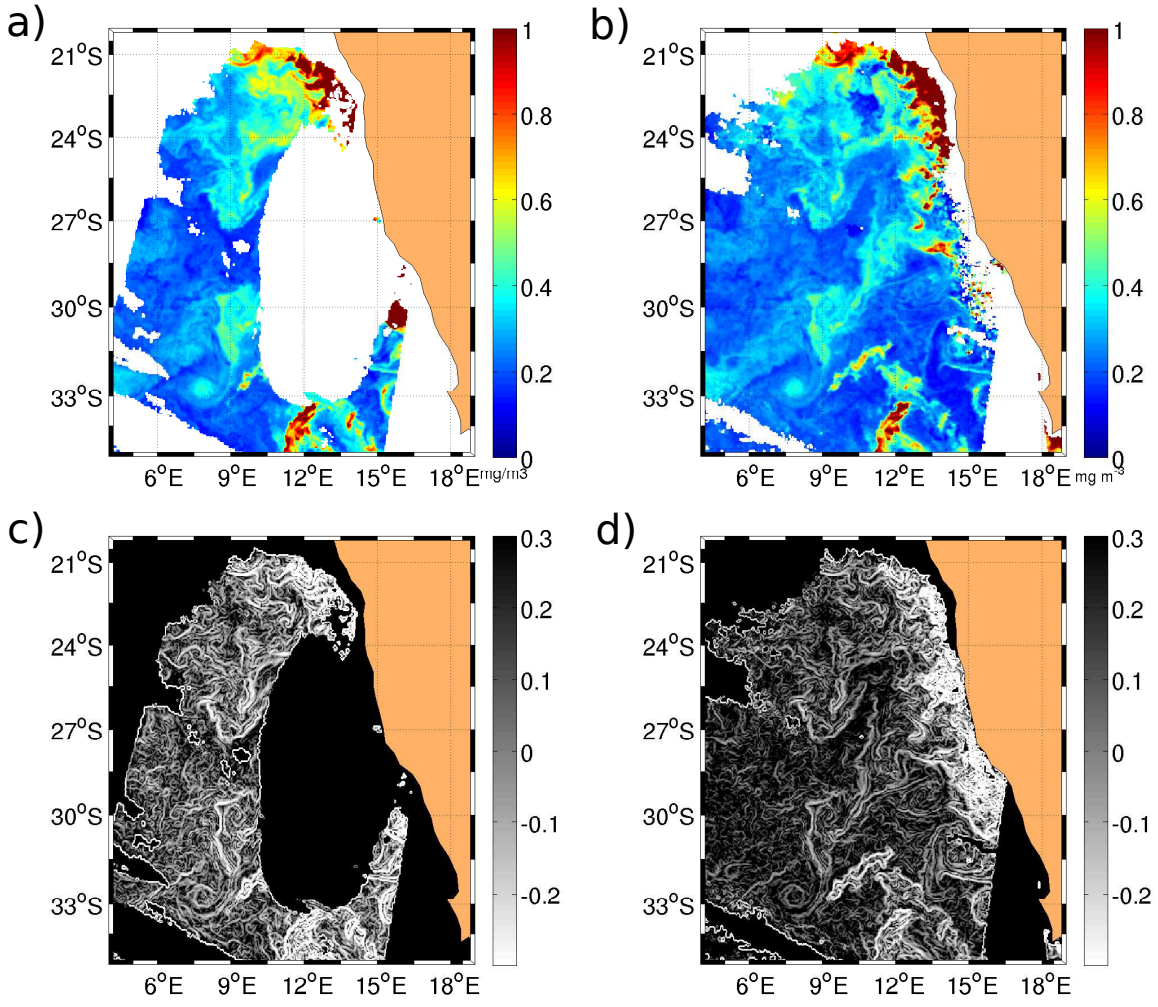

Fig. 2. Snapshot of Chl-a fields corresponding to September 21, 2006, regridded at 1/32° of spatial resolution from MERIS (a) and GSM GLOBCOLOUR (b). c) and d) are the spatial distribution of Singularity Exponents of the Chl-a plotted in a) and b) respectively

variables do not change when we zoom in or we zoom out the system, and can be represented by power-laws in particular, with the scaling exponents h.

It can be shown that the scaling exponents are the values taken on by localized singularity exponents, which can be computed at high precision in the acquired data using the Microcanonical Multifractal Formalism. Hence, within that framework, the multifractal hierarchy of turbulence, defined by a continuum of sets $\mathcal{F}_h$ indexed by scaling exponents h, is obtained as the level sets of the geometrically localized singularity exponents.

We will not review here the details in the computation of the singularity exponents $h(\mathbf{x})$, leaving the reader to consult references (Turiel et al., 2005, 2008; Pont et al., 2011b; Maji and Yahia, 2014; Sudre et al., 2015) for an effective description of an algorithm able to compute the $h(\mathbf{x})$ at every point $\mathbf{x}$ in a signal's domain.

Some examples of the singularity exponents of Chl and SST images for the different products described in Section 2.2 are shown in Fig. 2 c) and 2 d) and Fig. 3 c) and 3 d), respectively. As compared to the corresponding images of Chl and SST showed in Fig. 2 a) and 2 b) and Fig. 3 a) and 3 b), one can see the ability of the singularity exponents to unveil the cascade structures arisen by tracer-gradient variances hidden in satellite images.

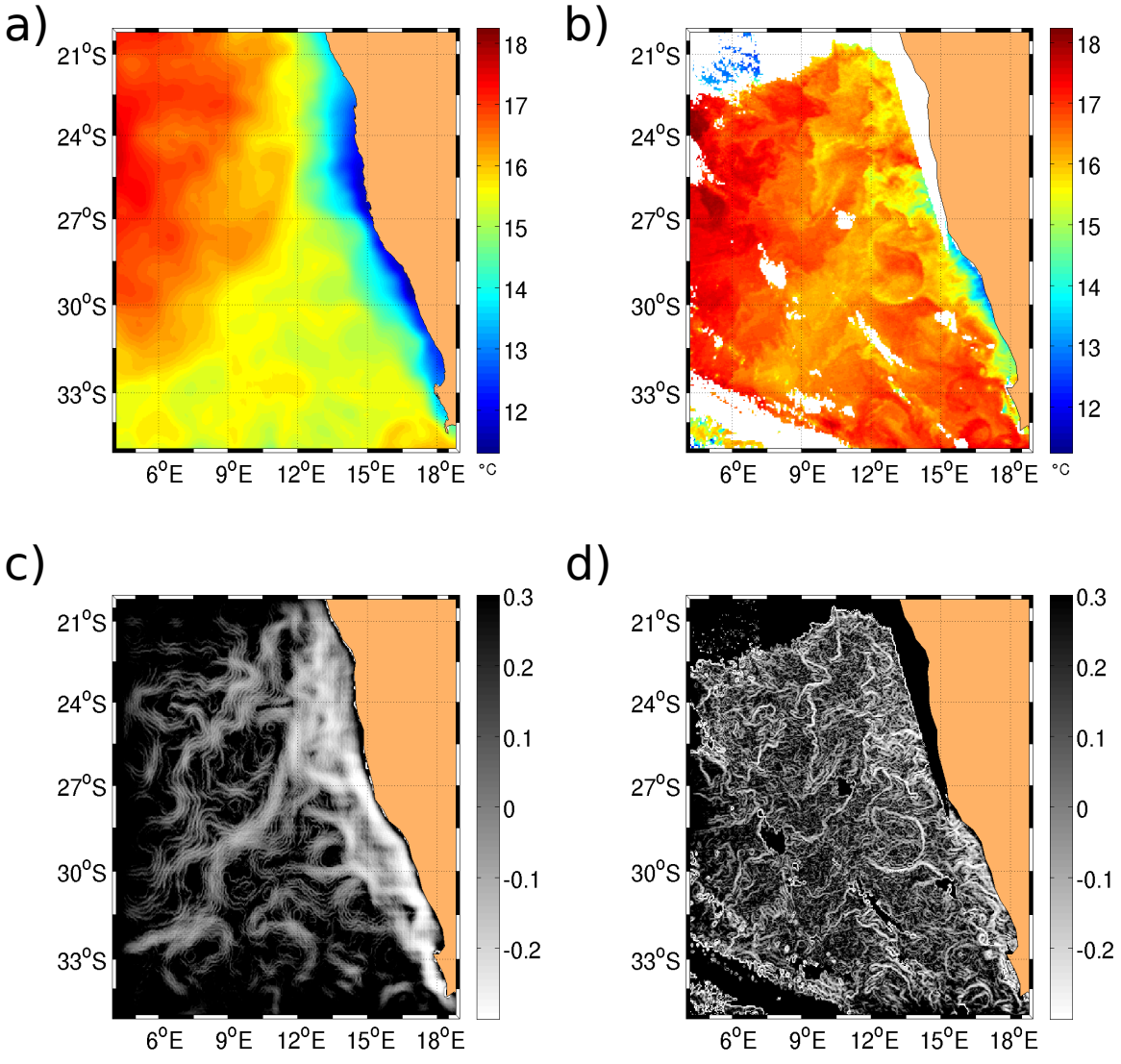

Fig. 3. Snapshot of SST fields corresponding to September 21, 2006 regridded at 1/32° of spatial resolution from OSTIA (a) and MODIS (b). c) and d) are the spatial distribution of Singularity Exponents of the SST plotted in a) and b) respectively.

3.2 Functional dependencies between the singularity exponents of intensive physical variables

Another important idea implemented in the methodology is the coupling of the physical information contained in SST and OC images with the ocean pCO_2. For instance, it is known, that marine primary production is a key process in the oceanic carbon cycling, and variations in the concentration of phytoplankton biomass can be related to variations in the carbon concentrations. Surface temperature is also related with the gas solubility in the ocean, and areas with high temperatures are more suitable for releasing CO_2 to the atmosphere. We have studied the relationship of SST and Chl-a variables with pCO_2 using the outputs of a coupled Regional Ocean Modeling System (ROMS) with the BIOgeochemical model of the Eastern Boundary Upwelling System (BIOEBUS) (Gutknecht et al., 2013). The ROMS includes several levels of nesting and composed grids, which makes it an ideal model for the basis of our methodology in working in two spatial resolutions. BIOEBUS has been developed for the Benguela to simulate the first trophic levels of the Benguela ecosystem functioning and also to include a more detailed description of the complete nitrogen cycle, including denitrification and anammox processes as well as the

oxygen cycle and the carbonates system. This model coupled to ROMS has been also shown to be skillful in simulating many aspects of the biogeochemical environment in the Peru upwelling system (Montes et al., 2014). When one compares SST and Chl with pCO_2 one finds undetermined functional dependency. However, when comparing their corresponding singularity exponents one obtains a clear simpler dependency. This is due to the fact that SST, Chl and pCO_2 are variables of different dimensions while singularity exponents are dimensionless quantities.

These results show that there is a good correlation between the turbulent transitions given by the singularity exponents and that singularity exponents are good candidates for a multiresolution analysis performed on the three signals SST, Chl and pCO_2. Furthermore, they studied the log-histograms and singularity spectrum to show that singularity exponents of pCO_2 images possess a multifractal character. Therefore, such signals are expected to feature cascading, multiscale and other characteristic properties found in turbulent signals as described in Turiel et al. (2008) and Arneodo et al. (1995). Consequently the use of non-linear and multiscale signal processing techniques is justified to assess the properties of the pCO_2 signal along the scales.

Therefore, in our methodology, the local connection between different tracer concentrations, i.e., SST, Chl-a with pCO_2, in order to obtain a proxy for pCO_2 at high resolution, is performed by using the following linear combination of multiple linear regressions:

$$\begin{aligned}\mathcal{S}(pCO_2)(\mathbf{x}) =& a(\mathbf{x})\mathcal{S}(SST)(\mathbf{x}) + b(\mathbf{x})\mathcal{S}(Chl\ a)(\mathbf{x}) + \\ & c(\mathbf{x})\mathcal{S}({pCO_2}^{LR})(\mathbf{x}) + d(\mathbf{x}),\end{aligned} \tag{3}$$

where $\mathcal{S}(pCO_2)(\mathbf{x})$ refers to the singularity exponent of pCO_2 at $\mathbf{x}$, $\mathcal{S}(SST)(\mathbf{x})$ to singularity exponent of SST at $\mathbf{x}$, $\mathcal{S}(Chl-a)(\mathbf{x})$ to singularity exponent of Chl-a signal at $\mathbf{x}$. In order to propagate the pCO_2 signal itself along the scales in the multiresolution analysis we introduce $\mathcal{S}({pCO_2}^{LR})$ to refer to the singularity exponent from pCO_2 at low resolution interpolated on the high resolution grid. $a(\mathbf{x})$, $b(\mathbf{x})$ and $c(\mathbf{x})$ are the regression coefficients associated to singularity exponents, and $d(\mathbf{x})$ is the error associated to the multiple-linear regression. These regression coefficients are estimated using simulated data from the ROMS-BIOEBUS model developed for the Benguela upwelling system and described above.

Once we have introduced these coefficients in the linear combination on satellite data, we obtain a proxy for singularity exponents of pCO_2 at high resolution and we can perform the multiresolution analysis to infer the information across the scales.

3.3 Cross-scale inference of pCO_2 data

Among the functional that are most commonly used to analyze the scaling properties of multifractal systems, wavelets occupy a prominent position. Wavelets projections are integral transforms that separate the relevant details of a signal at different scale levels, and since they are scale-tunable, they are appropriate to analyze the multiscale behavior of cascade processes and to represent them. However, as shown in Pottier et al. (2008),Yahia et al. (2010) and Pont et al. (2011a) not all multiresolution analyses are equivalent but the most interesting are those which are optimal with respect to inferring information along scales, in particular, in a context where information is to be propagated along the scales from low resolution to high resolution.

The effective determination of an optimal wavelet for a given category of turbulent signals is, in general, a very difficult open problem. This difficulty can be contoured by considering multiresolution analysis performed on the signal of the singularity exponents $h(\mathbf{x})$ themselves. Indeed, since the most singular manifold (the set $\mathcal{F}_h$ associated to the lowest singularity exponents) is associated with the highest frequencies in a turbulent signal, and since the multifractal hierarchy $\mathcal{F}_h$ converges to this set, it is physically evident that the multifractal hierarchy corresponds to a description of the detail spaces of a multiresolution analysis performed on a turbulent signal. Consequently, designing by V_j and W_j respectively the approximation and detail spaces computed on $\mathcal{S}(pCO_2)(\mathbf{x})$ signal, and by A_j and P_j their corresponding orthogonal projections from space $\mathbf{L}^2(\mathbb{R}^2)$, the following reconstruction formula:

$$A_{j-1}pCO_2 = A_j pCO_2 + P_j h \tag{4}$$

consists in reconstructing a signal across the scales using the detail spaces of the singularity exponents, hence regenerating a physical variable according to its cascade decomposition. From these ideas, which are described more fully in the paper by Sudre et al. (2015), we can deduce the following algorithm for reconstructing a super-resolution pCO_2 signal from available high-resolution SST, Chl-a, and low-resolution pCO_2:

i) After selecting a given area of study, compute the singularity exponents of SST, Chl and pCO_2 at low and high resolution from ROMS-BIOEBUS output. This is done once and then they can be used for every computation performed over the same area.

ii) Using Eq. 2 estimate ocean pCO_2 at low resolution: $p^{ocean}_{CO_2} = p^{air}_{CO_2} - F/\alpha K$, where:

- F: air-sea surface CO_2 fluxes provided by CarbonTracker product.
- K: gas transfer velocity obtained by the parametrization developed by Sweeney et al, 2007, as a function of the wind.
- α: gas solubility derived according to Weiss 1974.
- $p^{air}_{CO_2}$: provided by Globalview-CO2 product.

iii) Obtain the regression coefficients a, b, c and d of Eq. 3 for the singularity exponents obtained in step ii)

iv) Calculate the singularity exponents of available satellite SST, Chl at high resolution and ocean pCO_2 at low resolution (step i).

v) Use coefficients obtained in step iii) and apply Eq. 3 to the singularity exponents from satellite data (step iv) to estimate a proxy of singularity exponents of high resolution ocean pCO_2, $S(pCO_2)$.

vi) Using Eq. 4 reconstruct pCO_2 at high resolution from the multiresolution analysis computed on signal $S(pCO_2)$ and cross-scale inference on pCO_2 at low resolution.

vii) Use Eq. 2 to calculate air-sea CO_2 fluxes from the inferred pCO_2 obtained in step vi)

The methodology has been successfully applied to dual ROMS simulation data at two resolutions, obtaining a mean absolute error of pCO_2 reconstructed values with respect to ROMS simulated high-resolution pCO_2 equal to 3.2μatm (0.89% of relative error) (V. Garçon 2014, pers. comm.).

4 Preliminary analysis of Sea Surface Temperature (SST) and Chlorophyll images

Since the key element for the application of our inferring algorithm relies on the ability in obtaining the singularity exponents and their quality, the success of our methodology applied to satellite data depends on the quality and the properties of the input data. In order to assess such properties we perform a statistical analysis of the different datasets. First, we analyze the Chl and SST Probability Distribution Functions (PDFs). In Fig. 4a) we present the PDFs for Chl from MERIS, GLOBCOLOUR-GSM and GLOBCOLOUR-AVW; the required histograms are built using daily Chl values over 2006 and 2008 at each point of the spatial grid in the area of Benguela. Each one of these PDFs is broad and asymmetric, with a small mode (i.e. the value of Chl at which the probability reaches its maximum) between 0.1 and 0.2 mg/m^3 and a heavy tail. The heavy tail (i.e. non-gaussianity) means that the extreme values can not be neglected. In this case Chl values are mostly low (small mode) but there is a significant number of isolated and dispersed patches with very high Chl values producing intermittency (long tails in the PDF). Intermittency in the context of turbulence is the tendency of the probability distributions of some quantities to develop long tails, i.e. the occurrence of very extreme events.

Further information can be obtained by computing statistical quantities such as standard deviation, skewness and kurtosis. Table 1 shows that standard deviation is rather the same for the three OC products while skewness and kurtosis values hugely differ. The degree of intermittency is measured by the kurtosis, the higher the kurtosis, the higher the intermittency. We found that kurtosis is almost ten times higher in GLOBCOLOUR products than in MERIS.

We have repeated the same analysis for SST datasets. The PDFs of the SST values for OSTIA and MODIS products are shown in Fig. 4b). In this case both PDFs possess similar shape, broad with the mode around 18°C with a much less deviation from gaussianity as compared to Chl values. This is confirmed with the computation of the statistical moments showed in Table 1. We obtain small values of the standard deviation and kurtosis in both cases, although slightly higher in the case of MODIS. The kurtosis is less than 3, meaning that there is not an important number of atypical values of SST and therefore weak and short tails in the PDFs.

PRODUCT	Standard Deviation	Skewness	Kurtosis
MERIS	0.116 mg/m^3	2.6	21.9
GLOBCOLOUR-AVW	0.122 mg/m^3	4.7	204.6
GLOBCOLOUR-GSM	0.123 mg/m^3	5.3	215.4
OSTIA	1.97°C	-0.05	1.9
MODIS	2.11°C	-0.17	2.6

Table 1. Values of the standard deviation, skewness and kurtosis for the different products.

If turbulence is dominated by coherent structures localized in space and time, then PDFs are not Gaussian, and the kurtosis will be higher than 3. To analyze this feature we turn to the statistical analysis of the singularity exponents, which, as explained before, have the ability to unveil the cascade structures given by the tracer gradients. In Fig. 4c), it can be seen that the PDFs of the singularity exponents of the Chl for the three products are rather similar with almost the same standard deviation and with a slightly higher value of the kurtosis in the GLOBCOLOUR-GSM product, 4.3, than for MERIS, 3.1, and GLOBCOLOUR-AVW, 3.1, (see Table 2). This shows that Chl from GLOBCOLOUR-GSM product contains more extreme values which produce intermittency likely given by the strongest structures. The PDFs of the singularity exponents of the SST for OSTIA is narrower and with a highest peak than for MODIS SST. However, surprisingly the kurtosis is larger for singularity exponents of OSTIA SST, 5.1, than for MODIS SST, 3.2.

PRODUCT	Standard Deviation	Skewness	Kurtosis
MERIS	0.32 mg/m^3	0.59	3.1
GLOBCOLOUR-AVW	0.36 mg/m^3	0.40	3.1
GLOBCOLOUR-GSM	0.35 mg/m^3	0.63	4.3
OSTIA	0.29°C	1.0	5.1
MODIS	0.32°C	0.5	3.2

Table 2. Values of the standard deviation, skewness and kurtosis of the singularity exponents for the different products.

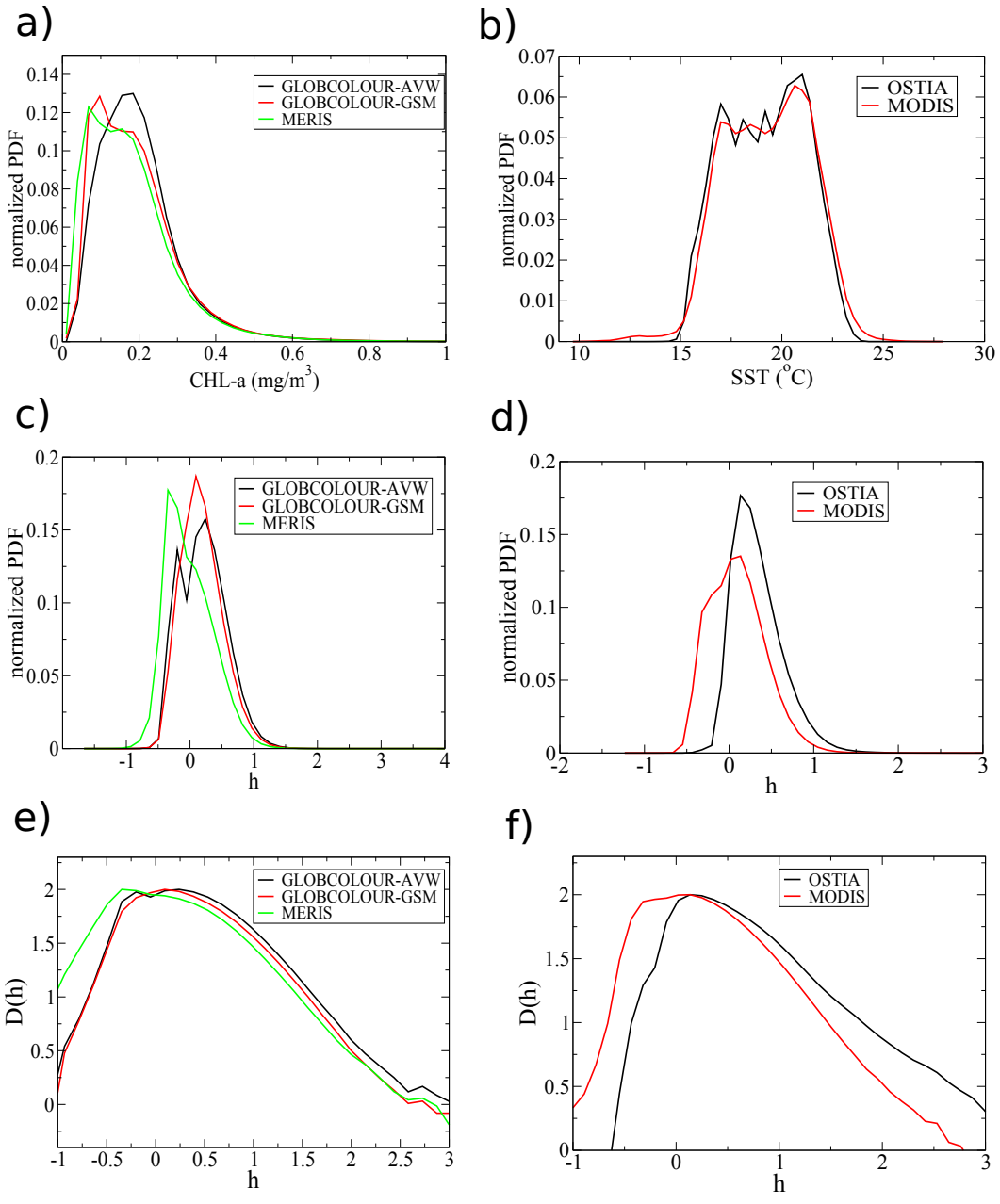

Fig. 4. a) Probability distribution functions (PDF) of Chl-a values derived from the three products: MERIS, GLOBCOLOUR-AVW and GLOBCOLOUR-GSM. (b) PDF of SST values for OSTIA and MODIS products. c) PDFs for the singularity exponents of Chl for the different Ocean Colour products. d) PDFs for the singularity exponents of Chl for the different SST products. e) Singularity spectra corresponding to c). f) Singularity spectra corresponding to d).

Finally, we obtain the singularity spectra from the empirical distributions of singularity exponents shown in Fig. 4c) and d). One can see in Fig. 4e) that for the two GLOBCOLOUR products the shape of the spectrum is closer to binomial cascade of multiplicative processes than for MERIS (we will come back to this discussion in more depth in next sections).

5 Results

5.1 Inference of super-resolution pCO_2 and air-sea fluxes of CO_2 offshore of the Benguela upwelling system

We now apply the methodology to infer ocean pCO_2 maps at super-resolution from pCO_2 at low resolution derived from CarbonTracker data (see Section 2) in the offshore area of the Benguela region.

From now on we are going to use the following notation for the three different sources of pCO_2: we refer to the values of ocean pCO_2 derived from CarbonTracker as $\mathrm{pCO_2^{Ctrack}}$, values of inferred pCO_2 at higher resolution from pCO_2 at low resolution together with computation of the cascade onto SST and chlorophyll-a concentration as $\mathrm{pCO_2^{infer}}$, and finally $\mathrm{pCO_2^{insitu}}$ refers to the values of the in-situ measurements of pCO_2.

For the inference we use the following three combinations of Chl and SST products described in Section 2.1: MERIS-OSTIA, GLOBCOLOUR-OSTIA, GLOBCOLOUR-MODIS. We do not include the MERIS-MODIS combination in the analysis due to the fact that the use of such satellite data results in a too drastic reduction of the coverage of the resulting $\mathrm{pCO_2^{infer}}$ field, but using merged products offers wider coverage instead. The inferred pCO_2 obtained from two merged products for Chl-a, GLOBCOLOUR GSM and GLOBCOLOUR AVW is rather the same, with a slightly improvement when GSM is used. Thus for the sake of clarity, we only show Figures for GLOBCOLOUR-GSM and some statistical results making comparisons with AVW. Therefore from now on we refer GLOBCOLOUR to the Chl-a obtained by the GSM merged method.

Figure 5d shows one example of $\mathrm{pCO_2^{infer}}$ field corresponding to March 22, 2006 when we use SST data from OSTIA (Fig. 5a), Ocean Colour from GLOBCOLOUR (Fig. 5b) at high resolution and pCO_2 at low resolution (Fig. 5c) derived from CarbonTracker air-sea flux of CO_2 (Fig. 5e) and using the Eq. 2. The air-sea flux of CO_2 at super-resolution (Fig. 5f) is obtained from the $\mathrm{pCO_2^{infer}}$ field and a constant value of atmospheric pCO_2 equal to 385.6μatm. On this day the images of the $\mathrm{pCO_2^{infer}}$ and fluxes of CO_2 combine a good coverage and a clear identification of small scale structures and gradients, as described below. Note that the air-sea CO_2 flux from CarbonTracker presents a large land mask close to the coast and consequently, we will rather study the offshore area of the Benguela upwelling. Comparing the figures one can see that values of pCO_2 and CO_2 flux over the domain (from 4.5°E to coast (taking out the mask of the CarbonTracker domain and from 20.5°S to 35°S) vary between 360 and 380μatm and between -4x10^{-8} and 0.5x10^{-8} mol C m^{-2} s^{-1}, respectively. The resultant flux of CO_2 is positive (towards the atmosphere) in the region 25°-28°S and from 7°E eastward to the coast and is negative (into the ocean) south of 30°S and east of 6°E. Thus, we see that in the southern part of the Benguela area there is a strong CO_2 sink and the northern part behaves as a weak CO_2 source.

What is new in the reconstructed pCO_2 is, for instance, that the cascade of information across the scales enhances gradients in the field of pCO_2. It is striking that the high-resolution map provides the position of the North-South dipole "front" located at 30°S (i.e. -1.5x10^{-8} isoline in green) which could not be inferred accurately from the low resolution map. The low resolution map would provide an estimate of the location of the "front" that is $\sim$1.5° northern of the location inferred from the high-resolution map. Moreover one can see small structures in the $\mathrm{pCO_2^{infer}}$ field between 33-35°S and 9-12°E in the $\mathrm{pCO_2^{infer}}$ field (Fig. 5d) . The small spatial scale variability is captured in the super-resolution pCO_2 field and not in $\mathrm{pCO_2^{Ctrack}}$ as shown in the longitudinal profile of the images plotted in Fig. 5 at latitude 33.5°S (see Fig. 6). The same high spatial variability given by the small scale structures of the SST and OC images can be appreciated in their corresponding longitudinal profiles displayed in the panel a) and b) of Fig. 6. It is worthy to note the change in the shape of the profiles between the $\mathrm{pCO_2^{infer}}$ and $\mathrm{pCO_2^{Ctrack}}$ and fluxes of CO_2 at large scale, from 5.5°E to 10.5°E, showing that the method not only introduces small scale features but also modifies the large scale spatial variability.

5.2 Evaluation of using different satellite products

Since the underlying aim of this work is to develop a methodology to infer super-resolution pCO_2 from space using remote observations, we perform a validation study of the different data used in the inferring computations. This provides us an evaluation of which satellite products are more suitable for our methodology and thus a gain in confidence in our method as well as a better understanding of its limitations. The evaluation analysis is addressed taking into account two main concerns: one related to the number of valid points yielded in the $\mathrm{pCO_2^{infer}}$ field, and another with regard to the degradation of the information contained in the transition fronts. A valid point is a pixel where we have simultaneously Chl, SST and pCO_2 values from CarbonTracker, from which we can obtain a value of $\mathrm{pCO_2^{infer}}$, in other words without missing information. One example comparing the reconstructed pCO_2 field obtained from the mentioned above three products combinations is plotted in Fig. 7. The general pattern is quite similar in all of them with some differences in the details of the small scales and in the missing points due to cloudiness (white patches). This example clearly shows how different coverage of the pCO_2 can be in the field depending on the products combination.

Similar results are found when one compares the spatial distribution of time average over 2006 and 2008 of the $\mathrm{pCO_2^{infer}}$ values for the three product combinations (Fig 8). The same pattern with an area of higher pCO_2 between 24°S and 30°S and lower pCO_2 values outside this region is pro-

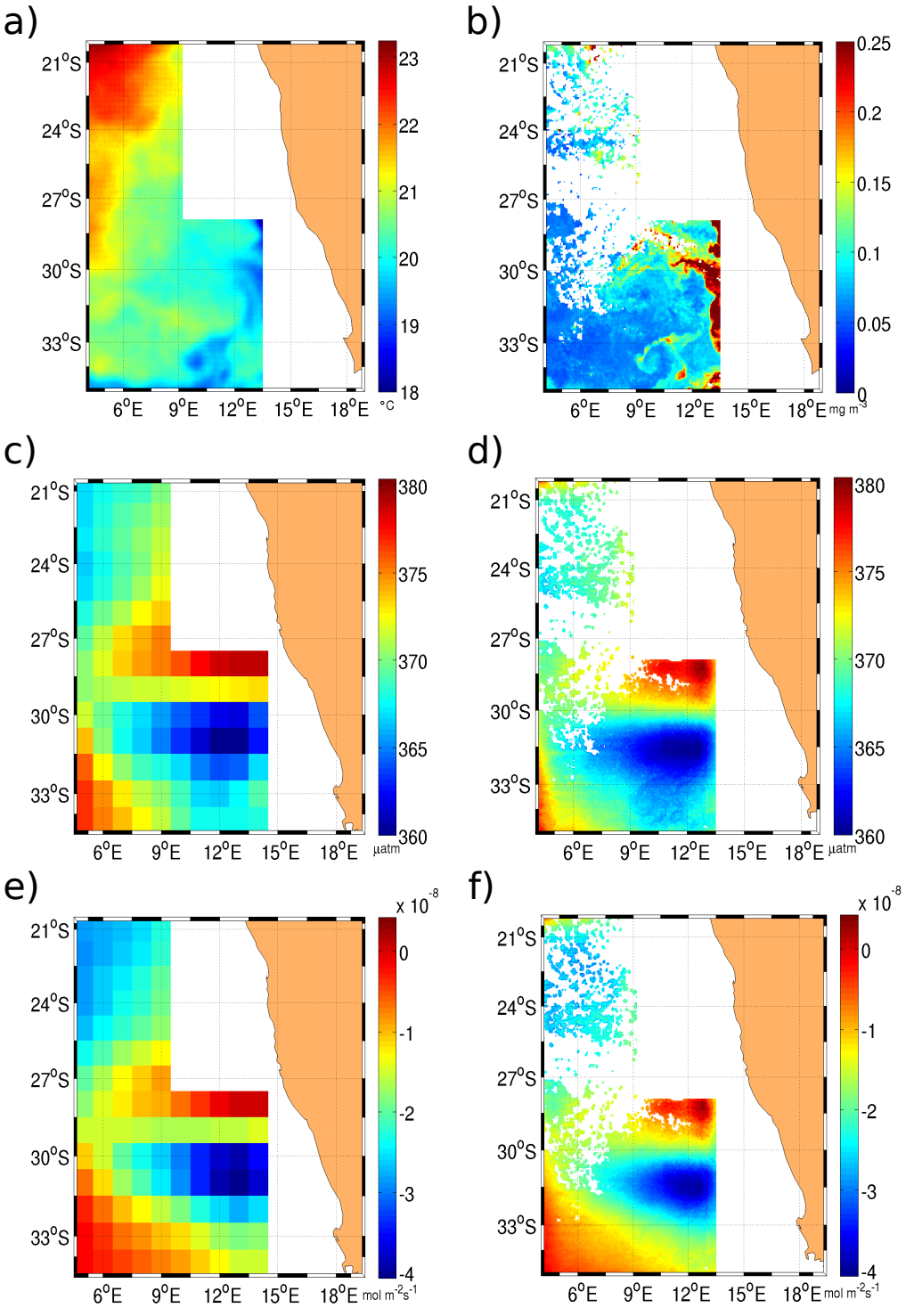

Fig. 5. Maps of a) SST from OSTIA at 1/32° of spatial resolution, b) Chl at 1/32° of spatial resolution from GSM GLOBCOLOUR products, c) ocean pCO_2 from CarbonTracker at the spatial resolution of 1°, d) inferred pCO_2 at super-resolution (1/32°) derived from OSTIA SST and GLOBCOLOUR-GSM Chl-a shown in a) and b) respectively, e) Air-sea CO_2 flux as derived from CarbonTracker and f) Air-sea CO_2 flux computed from super-resolution pCO_2 shown in d) at 1/32°. All images correspond to March 22, 2006. White color corresponds to invalid pixels due to cloudiness and points inside of the CarbonTracker land mask

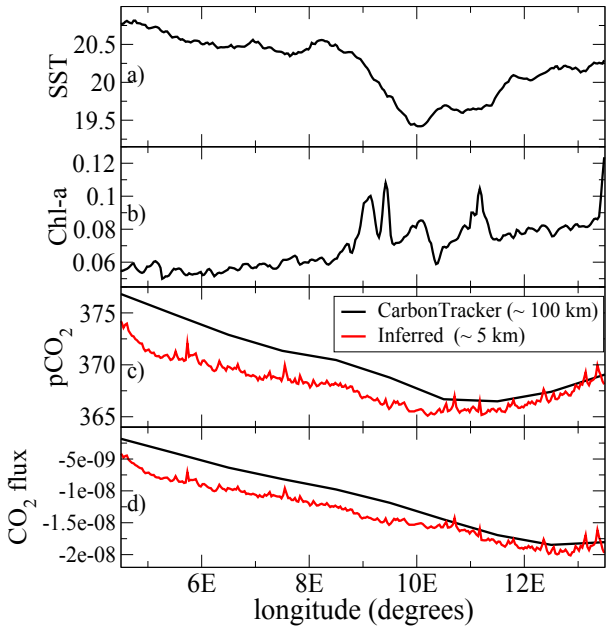

Fig. 6. Longitudinal profiles of a) SST from OSTIA products in units of °C, b) Chl from GLOBCOLOUR-GSM ocean in mg/m^3, c) $\mathrm{pCO_2^{Ctrack}}$(black line) and $\mathrm{pCO_2^{infer}}$(red line) in μatm, and d) air-sea CO_2 fluxes from CarbonTracker (black line) and inferred air-sea CO_2 fluxes (red line) in mol C m^{-2} s^{-1}. All these longitudinal profiles correspond to the fixed latitude equal to 33.5°S of the plots shown in Fig. 5 for March 22, 2006.

duced with the three combinations. The most noticeable differences are located in the most northern region and in the south-eastern region off Benguela. This can be quantified by computing the standard deviation of the reconstructed $\mathrm{pCO_2}$ values among the different combination of datasets. Fig. 8 d) shows the spatial distribution of the time average over 2006 and 2008 of the standard deviation computed in each pixel among the $\mathrm{pCO_2^{infer}}$values obtained from the three products combinations. The larger values of the dispersion (not greater than 5μatm) are found in the northern region from 23°S to the north and and in the southern region, in particular, in the area from 31.5 °S to the south and from 11°E to the east. The low value of the dispersion indicates that the method is robust when different datasets are used in the inference.

First, we compute the number of valid points in the $\mathrm{pCO_2^{infer}}$field for each product combination. Table 3 summarizes the total number of valid points for each products combination for both years 2006 and 2008. As expected, the number of valid points is found to be the highest for the combination of merged products OSTIA SST and GLOBCOLOUR-GSM with N_{GO}=27313043 points, followed by the combination MODIS SST and GLOBCOLOUR Chl with N_{MG}=20397047 points and finally by the OSTIA SST and MERIS Chl combination with

Valid Points in the inferred $\mathrm{pCO_2}$ fields: 2006/2008	
Nb total pixels domain	55711378
Nb Points OSTIA-MERIS	9800776
Nb Points OSTIA-GLOBCOLOUR(AVW)	26382072
Nb Points OSTIA-GLOBCOLOUR(GSM)	27313043
Nb Points MODIS-GLOBCOLOUR(GSM)	20397047
Proportion OSTIA-GSM/OSTIA-MERIS	2.78
Proportion OSTIA-GSM/MODIS-GSM	1.33
Proportion MODIS-GSM-/OSTIA-MERIS	1.08
LP_{OM}	82%
LP_{OG}(AVW)	53%
LP_{OG}(GSM)	51%
LP_{MG}	63%

Table 3. Number of valid points in the $\mathrm{pCO_2}$ fields and their difference between the three combinations of MERIS or GLOBCOLOUR CHL with OSTIA or MODIS SST in the area of Benguela.

N_{OM}=9800776 points. Looking at the different proportions, we find that the number of valid points is 2.78 times larger when using the merged products OSTIA and GLOBCOLOUR-GSM than using OSTIA and MERIS, 1.33 times larger than using MODIS and GLOBCOLOUR-GSM and 1.08 times larger using OSTIA SST and GSM Chl-a than using MODIS SST and GSM Chl a. Further, if we know that the total number of pixels in the domain taking out the points of the CarbonTracker mask and for the two years is N_p=55711378, one can estimate the loss of valid points for each combination, LP_x. LP_x is computed by dividing the relative difference between the number of total available pixels in the domain N_p and the number of points in the inferred pCO_2 field obtained for each product combination,N_x, with respect to the total number of pixels N_p, $LP_x = \frac{N_p - N_x}{N_p} 100\%$. Here the subscript x refers to the product combination (e.g. LP_x = LP_{OM}, LP_{OG} and LP_{MG} for the loss of valid points with the OSTIA-MERIS, OSTIA-GLOBCOLOUR and MODIS-GLOBCOLOUR products combination, respectively). The loss of valid points due to cloudiness in the ocean colour and SST images is less severe for the OSTIA-GLOBCOLOUR combination with a loss of 51% and being the more affected by the cloudiness the OSTIA-MERIS combination with a loss of 82%.

Next we explore the quality of the information contained in the transition fronts, in particular, in the non-merged products such as MERIS OC and MODIS SST as compared to the merged products: GLOBCOLOUR OC and OSTIA SST. The PDFs of $\mathrm{pCO_2}$ values from CarbonTracker and $\mathrm{pCO_2^{infer}}$values for the three combinations of OC and SST products, i.e. MERIS-OSTIA, GLOBCOLOUR-OSTIA, MODIS-GLOBCOLOUR (see Fig. 9) show that there is a good correspondence of all $\mathrm{pCO_2^{infer}}$values with those from $\mathrm{pCO_2^{Ctrack}}$. Indeed the histograms show also a better

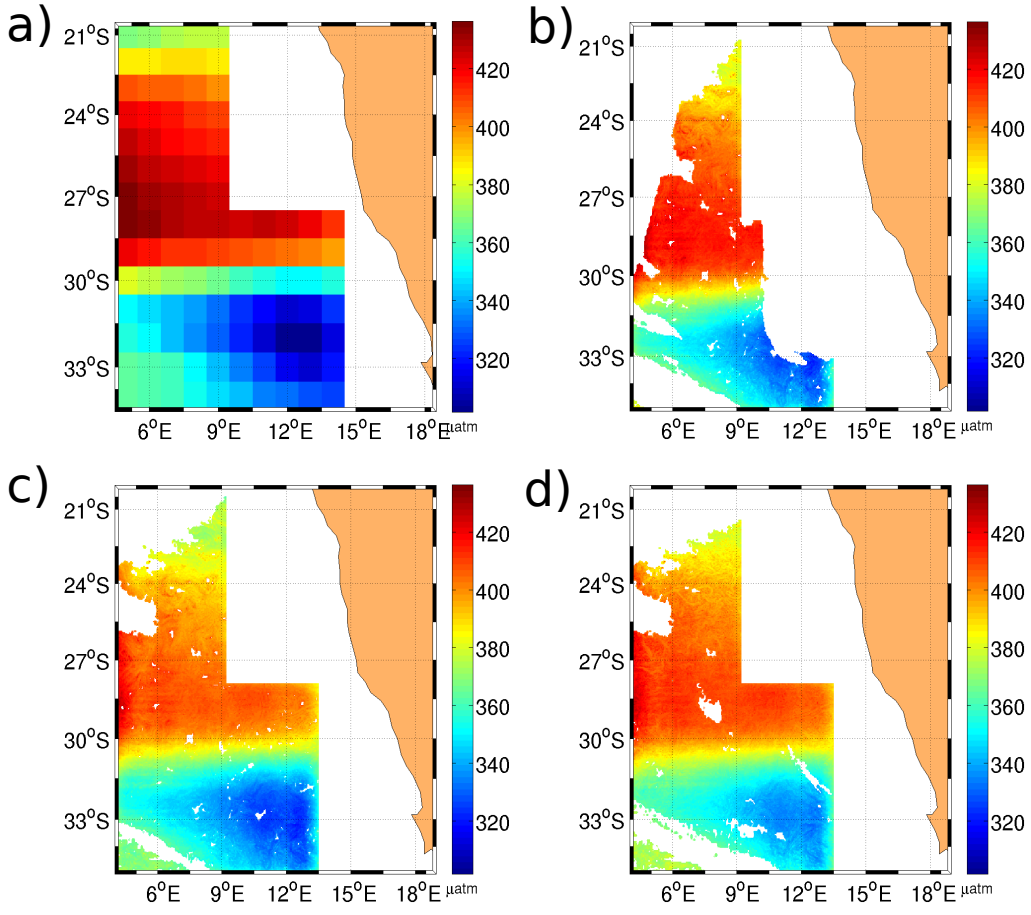

Fig. 7. a) Map of pCO_2 field at low resolution from CarbonTracker. Reconstructed pCO_2 field at super-resolution using: b) OSTIA SST and MERIS Chl-a, c) OSTIA SST and GSM-GLOBCOLOUR Chl-a and d) MODIS SST and GSM-GLOBCOLOUR Chl-a. All maps correspond to September 21 2006.

agreement between merged products and CarbonTracker: the peak of the PDF for pCO_2^{infer} is closer to CarbonTracker peak in the case of OSTIA and GLOBCOLOUR than when using MERIS and MODIS products.

Furthermore, to analyze the realism of the transitions fronts for the different products we compute the singularity spectra for the three product combinations (see Figure 10). One can see that at low values of h (singularity exponent), related to the most singular manifolds, the shape of singularity spectrum for inferred data from merged products better matches a binomial cascade, with an improved description of the dimension of the sharpest transition fronts. We know from the theory, that tracers advected by the flow in the turbulent regime, as it happens in the ocean, shows a multifractal behavior with a characteristic singularity spectrum $D(h)$ similar, for some types of turbulence, to $D(h)$ for the binomial multiplicative process.

5.3 Validation with in-situ measurements

Next, we perform a validation analysis of the results of our algorithm to infer pCO_2 at super-resolution with field observations of oceanic pCO_2. In particular we perform the validation using pCO_2 ocean data from in-situ measurements (pCO_2^{insitu}) taken in the Benguela region (see Section 2.3). We decided to carry out directly the validation on pCO_2 rather than on the air-sea CO_2 flux since the field measurements do provide oceanic pCO_2 data.

An example of the qualitative comparison of values of pCO_2^{Ctrack}, pCO_2^{infer} for all the products combinations and pCO_2^{insitu} at the intersections of the QUIMA cruise during July 4-7th, 2008, as a function of the longitudinal coordinate

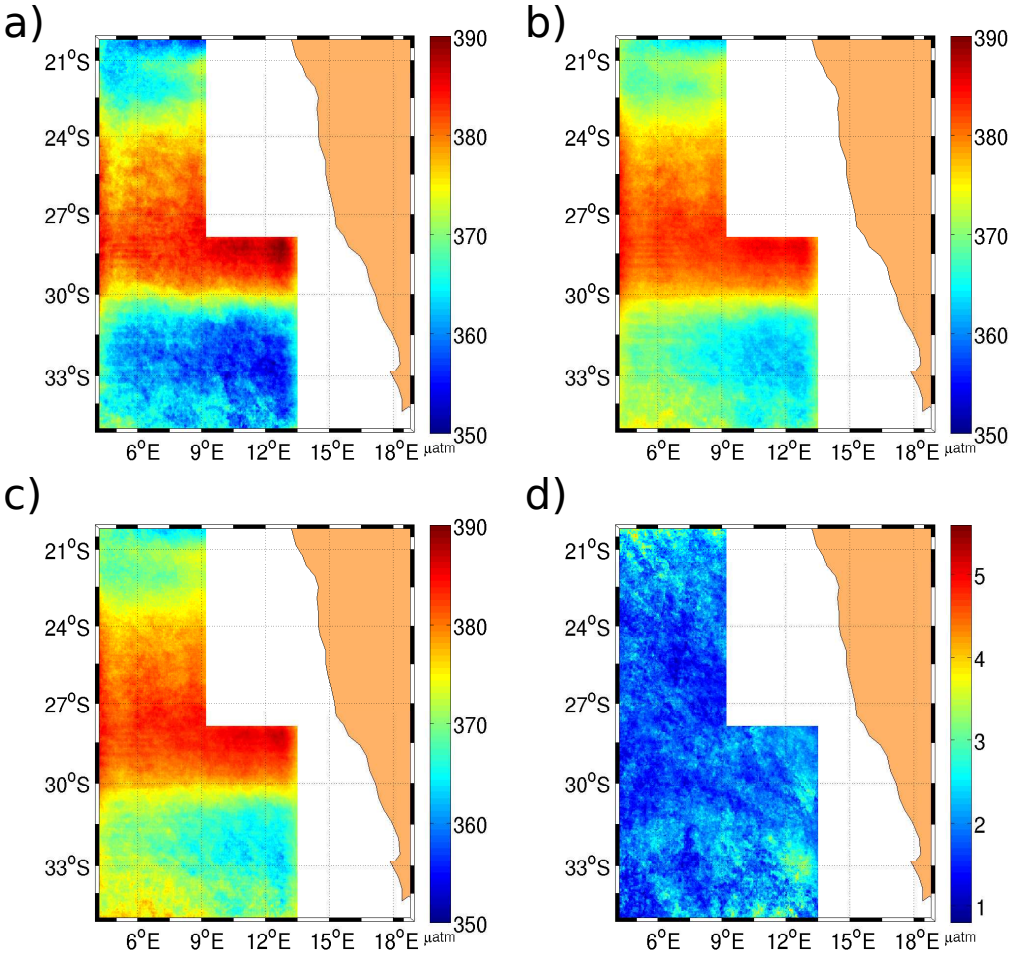

Fig. 8. Spatial distribution of the time average over both 2006 and 2008 years of the pCO_2^{infer} values using: a) OSTIA SST and MERIS Chl-a, b) OSTIA SST and GSM-GLOBCOLOUR Chl-a and c) MODIS SST and GSM-GLOBCOLOUR Chl-a. d) Map with spatial distribution of the standard deviation for the pCO_2^{infer} among the different combination of the datasets.

of the intersections, is shown in Figure 11. While there are visible differences between various pCO_2 values, the values of pCO_2^{infer} approximate better pCO_2^{insitu} values than those of pCO_2^{Ctrack}. The small scale patterns are well reproduced in the inferred pCO_2 field. Values of pCO_2^{infer} exhibit gradients and small scale fluctuations, likely induced by the presence of fronts, which can be also detected on the profile of the in situ measurements of pCO_2. Most of days pCO_2^{infer} and pCO_2^{Ctrack} values overestimate pCO_2^{insitu} values. In some days, pCO_2^{infer} values follow the same trend, with the same small scale fluctuations than pCO_2^{insitu}.

First, we analyze the number of valid intersections for each product combination. A valid intersection is a placement in space and time common to the inferred, CarbonTracker and in-situ pCO_2, without missing values. On one hand, among the 20 available cruises in the Benguela through 2005, 2006 and 2008 we find that the total number of in-situ measurements in the Benguela region under study is $N_{\rm insitu}$=17355 and within the CarbonTracker domain this number is reduced to $N_{\rm Ctrack}$= 8377 measurements. To estimate the loss of valid intersections due to the land mask of of the CarbonTracker we compute the relative difference of the number of intersections between the cruise trajectories and the CarbonTracker domain with respect to the number of the in-situ measurements, $L_{\rm Ctrack} = \frac{N_{\rm insitu} - N_{\rm Ctrack}}{N_{\rm insitu}} 100\% = 52\%$, showing that half of the measurements fall within the coastal region of the Benguela (land masked by CarbonTracker).

The number of valid intersections is the largest with the OSTIA-GLOBCOLOUR combination (Table 4). To quantify the loss of valid intersections between the in-situ measurements and points in the pCO_2^{infer} field, likely due to

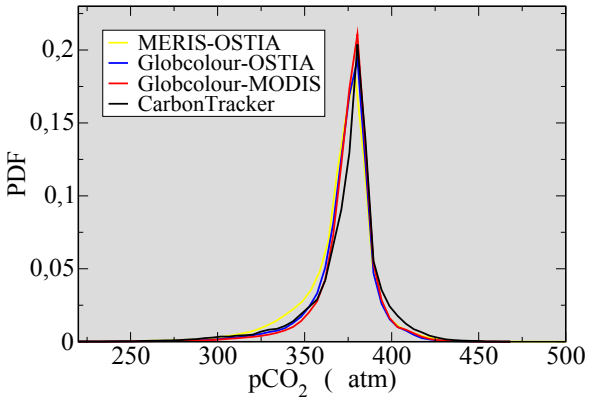

Fig. 9. Comparison of the Probability Distribution Functions of CarbonTracker and inferred pCO_2 values over the Benguela area for the three different SST and OC product combinations: MERIS Chl and OSTIA SST, GLOBCOLOUR merged Chl and OSTIA SST, and GLOBCOLOUR merged Chl and MODIS SST

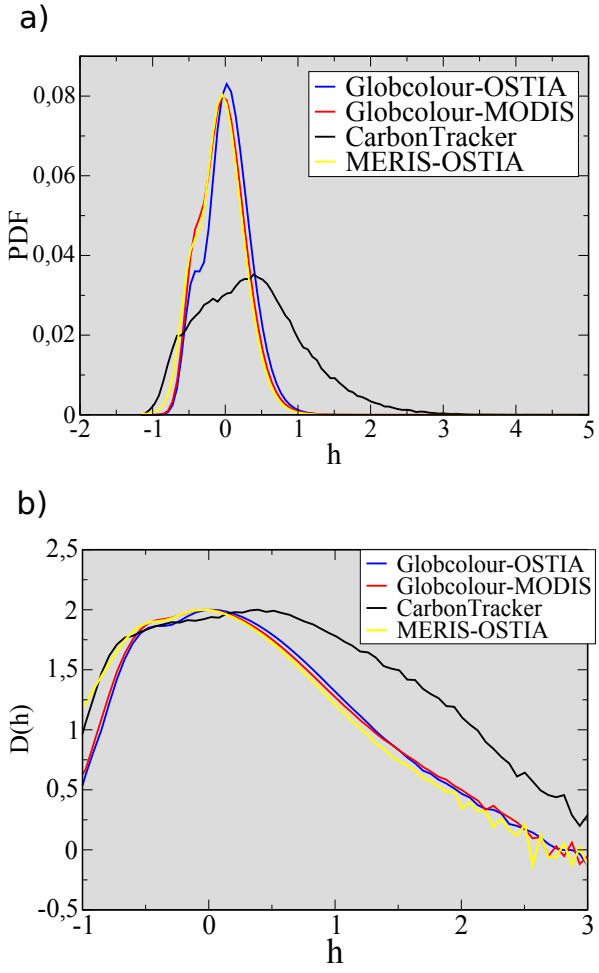

Fig. 10. a) Empirical PDFs for the singularity exponents of pCO_2 fields from CarbonTracker and from the cascade of the three product combinations. b) Associated singularity spectra. In these computations we use all the pCO_2 values obtained in 2006 and 2008.

the cloudiness, we compute the relative difference between the number of measurements into the CarbonTracker domain and the valid points in the inferred pCO_2 field with respect to the number of intersections measurements of each cruise and the pCO_2^{Ctrack} field, $L_{\rm infer} = \frac{N_{\rm Ctrack} - N_{\rm infer}}{N_{\rm Ctrack}} 100\%$. We repeat such a computation for the three product combinations. The percentage of losses of intersections in inferred field $L_{\rm infer}$ becomes twice as large than in the case of the OSTIA-SST and MERIS-Chl combination, and even higher than with the CarbonTracker domain mask.

In order to quantitatively study the difference between values of $\rm pCO_2^{Ctrack}$ and $\rm pCO_2^{infer}$ with respect to $\rm pCO_2^{insitu}$ measurements we compute the following statistical quantities:

– *Mean Difference (MD)*: average over all the intersections of the difference between $\rm pCO_2^{Ctrack}$, $\rm pCO_2^{infer}$ and $\rm pCO_2^{insitu}$ at the same intersection, i,

$$MD_{\rm Ctrack} = \frac{1}{N}\sum_{i=1}^{N}(pCO_2^{Ctrack}(i) - pCO_2^{insitu}(i)) \quad (5)$$

$$MD_{\rm infer} = \frac{1}{N}\sum_{i=1}^{N}(pCO_2^{infer}(i) - pCO_2^{insitu}(i)) \quad (6)$$

where N is the number of intersections.

– *Mean Absolute Error (AE)*: average over all the intersections of the absolute values of the difference between $\rm pCO_2^{Ctrack}$ or $\rm pCO_2^{infer}$ and $\rm pCO_2^{insitu}$ at the same intersection,

$$AE_{\rm Ctrack} = \frac{1}{N}\sum_{i=1}^{N}\left|pCO_2^{Ctrack}(i) - pCO_2^{insitu}(i)\right| \quad (7)$$

$$AE_{\rm infer} = \frac{1}{N}\sum_{i=1}^{N}\left|pCO_2^{infer}(i) - pCO_2^{insitu}(i)\right| \quad (8)$$

– *Mean Relative Error (RE)*: average over all the intersections of the errors of the estimated values of pCO_2 (CarbonTracker or inferred) with respect to the refer-

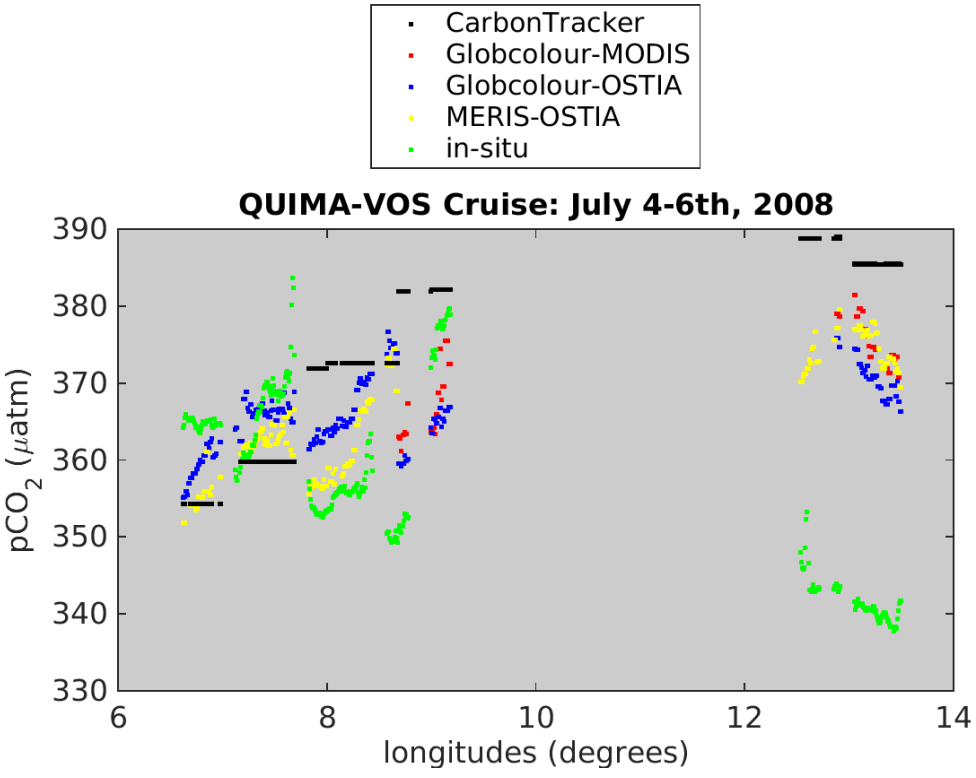

Fig. 11. Values of pCO_2^{Ctrack}(black points), pCO_2^{infer}(MODIS-SST/GLOBCOLOUR-Chl) (red points), pCO_2^{infer}(OSTIA-SST/GLOBCOLOUR-Chl) (blue points) pCO_2^{infer}(OSTIA-SST/MERIS-Chl) (yellow points) and pCO_2^{insitu}(green points) in the intersections as a function of latitude corresponding to the valid intersections during the QUIMA cruise through July 4-6th, 2008

ence pCO_2 values (in-situ) at the same intersection,

$$RE_{\text{Ctrack}} = \frac{1}{N}\sum_{i=1}^{N}\left|\frac{pCO_2^{Ctrack}(i) - pCO_2^{insitu}(i)}{pCO_2^{insitu}(i)}\right| \quad (9)$$

$$RE_{\text{infer}} = \frac{1}{N}\sum_{i=1}^{N}\left|\frac{pCO_2^{infer}(i) - pCO_2^{insitu}(i)}{pCO_2^{insitu}(i)}\right| \quad (10)$$

We started the statistical validation by analyzing each QUIMA cruise separately (not shown) and we found that in most of the cruises, the absolute error for inferred pCO_2 is relatively small (less than 15 μatm) except on August 21, 2006 and May 17, 2008 with an error of 44 μatm and 30 μatm, respectively. Then we address the global validation using all available cruises during these years.

We summarize in Table 4 the results of the computations of the errors given by Eq. 7 to Eq.10 by making averages over all valid intersections found during 2005, 2006 and 2008. The absolute error, AE is smaller in the three cases of pCO_2^{infer}(17.77, 16.47 and 16.62 μatm for OSTIA-MERIS, OSTIA-GLOBCOLOUR and MODIS-GLOBCOLOUR combinations, respectively) than for pCO_2^{Ctrack}(21.34, 22.08 and 22.07 μatm, respectively), showing the fact that the estimated pCO_2 field at super-resolution using our algorithm is improving the pCO_2 field obtained from CarbonTracker. The smallest AE is for the combination of SST and Chl provided by merged products. The values of $pCO_2^{Ctrack}$are, in average, larger than pCO_2^{insitu}(MD_{Ctrack}

	OST-MER	OST-GLOB	MOD-GLOB
Nb valid intersections	747	1928	1460
L_{infer} (%)	91	76	82
MD_{Ctrack} (μatm)	2.97	8.83	14.93
MD_{infer} (μatm)	0.15	3.42	8.42
AE_{Ctrack} (μatm)	21.34	22.08	22.07
AE_{infer} (μatm)	17.77	16.47	16.62
RE_{Ctrack}	0.059	0.060	0.061
RE_{infer}	0.048	0.045	0.046

Table 4. Mean error, absolute error and relative error of pCO_2 values obtained from CarbonTracker and pCO_2 values inferred at super-resolution with respect to values of pCO_2 measurements during the QUIMA2005/QUIMA2006/QUIMA2008 cruises in the Benguela region.

= 2.97, 8.83 and 14.93 μatm) while the differences between pCO_2^{infer} and pCO_2^{insitu} values compensate each other (MD_{infer} = 0.15, 3.42 and 8.42 μatm). In all cases the MD_{Ctrack} and MD_{infer} are positive, meaning that the pCO_2 values are overestimated. Finally, comparing the relative error of pCO_2^{Ctrack} and pCO_2^{infer} with respect to pCO_2^{insitu}, we found that the relative error is low in all cases, being smaller for pCO_2^{infer} than for pCO_2^{Ctrack}.

Finally, if we only compare the statistics errors at the common valid intersections between the pCO_2^{infer} using the three product combinations with pCO_2^{Ctrack} and with the in-situ measurements (see Table 5), we obtain 458 mutual intersections. We obtain similar results that when taking into account all the intersections. The absolute error is smaller in the case of pCO_2^{infer}, 17.65 μatm, than with pCO_2^{Ctrack}, 20.24 μatm, indicating that our algorithm is improving the estimation of ocean pCO_2. The smallest AE is again for the combination with merged products. MD is positive showing that the most of the time pCO_2^{infer} and pCO_2^{Ctrack} values are overestimated (It can be appreciated in Figure 11). Again the relative error is small, less than 0.06, for all the product combinations.

	OST-MER	OST-GLOB	MOD-GLOB
Nb valid intersections	458	458	458
MD_{Ctrack} (μatm)	8.01	8.01	8.01
MD_{infer} (μatm)	4.37	1.62	3.32
AE_{Ctrack} (μatm)	23.23	23.23	23.23
AE_{infer} (μatm)	19.92	16.31	18.85
RE_{Ctrack}	0.065	0.065	0.065
RE_{infer}	0.055	0.045	0.051

Table 5. Mean error, absolute error and relative error of pCO_2 values obtained from CarbonTracker and pCO_2 values inferred at super-resolution with respect to values of pCO_2 measurements during the QUIMA2005/QUIMA2006/QUIMA2008 cruises in the Benguela region at the same intersections.

6 Conclusions

In this work we have presented a method to infer high resolution CO_2 fluxes by propagating the small scales information given in satellite images across the scales of a multiresolution analysis determined on the critical transitions giving by singularity exponents. More specifically, we have reconstructed maps of CO_2 fluxes at high resolution (4 km) offshore of the Benguela region using SST and ocean colour data at this resolution, and CarbonTracker CO_2 fluxes data at low resolution (110 km). The inferred representation of ocean surface pCO_2 improves the description provided by CarbonTracker, enhancing the small scale variability. Spatial fluctuations observed in latitudinal profiles of in-situ pCO_2 have been also obtained in the inferred pCO_2, showing that the inferring algorithm is catching the small scales features of the pCO_2 field. The examination of different combinations of Ocean Colour and Sea Surface Temperature (SST) products reveals that using merged products, i.e. GLOBCOLOUR, the quality and the number of valid points in the pCO_2 field are increased. We have obtained that mean absolute errors of the inferred values of pCO_2 with respect to in-situ measurements are smaller than for CarbonTracker. The statistical comparison of inferred and CarbonTracker pCO_2 values with in-situ data shows the potential of our method as well as the shortcomings of using CarbonTracker data for the estimation of air-sea CO_2 fluxes. From these results it can be said that the outputs of our algorithm will only be as good as the inputs.

We are aware that further investigations can be performed in order to improve the algorithm. On one hand the multiple linear regression coefficients could be derived differentiating the seasons (i.e. coefficients would vary as a function of calendar month) considering the marked seasonal cycle in the Benguela upwelling system. Additionally, future works will be focused in the extension of the computations towards larger areas until being able to infer global high resolution CO_2 fluxes. This will allow us to perform an even more comprehensive and robust validation from in situ measurements since more in-situ measurements will be used to make the comparison.

Acknowledgements. This work is a contribution to ESA Support To Science Element Grant N° 400014715/11/I-NB OceanFlux-Upwelling Theme. The Surface Ocean CO_2 Atlas (SOCAT) is an international effort, supported by the International Ocean Carbon Coordination Project (IOCCP), the Surface Ocean Lower Atmosphere Study (SOLAS), and the Integrated Marine Biogeochemistry and Ecosystem Research program (IMBER), to deliver a uniformly quality-controlled surface ocean CO_2 database. The many researchers and funding agencies responsible for the collection of data and quality control are thanked for their contributions to SOCAT.

References

Abraham, E. and Bowen, M.: Chaotic stirring by a mesoscale surface-ocean flow, Chaos, 12, 373–381, 2002.

Abraham, E., Law, C., Boyd, P., Lavender, S., Maldonado, M., and Bowie, A.: Importance of stirring in the development of an iron-fertilized phytoplankton bloom, Nature, 407, 727, 2000.

Arneodo, A., Argoul, F., Bacry, E., Elezgaray, J., and J.F., M.: Ondelettes, multifractales et turbulence, Diderot Editeur, Paris, France, 1995.

Bakker, D. C. E., Pfeil, B., Smith, K., Hankin, S., Olsen, A., Alin, S. R., Cosca, C., Harasawa, S., Kozyr, A., Nojiri, Y., O'Brien, K. M., Schuster, U., Telszewski, M., Tilbrook, B., Wada, C., Akl, J., Barbero, L., Bates, N. R., Boutin, J., Bozec, Y., Cai, W.-J., Castle, R. D., Chavez, F. P., Chen, L., Chierici, M., Currie, K., de Baar, H. J. W., Evans, W., Feely, R. A., Fransson, A., Gao, Z., Hales, B., Hardman-Mountford, N. J.,

Hoppema, M., Huang, W.-J., Hunt, C. W., Huss, B., Ichikawa, T., Johannessen, T., Jones, E. M., Jones, S. D., Jutterström, S., Kitidis, V., Körtzinger, A., Landschützer, P., Lauvset, S. K., Lefèvre, N., Manke, A. B., Mathis, J. T., Merlivat, L., Metzl, N., Murata, A., Newberger, T., Omar, A. M., Ono, T., Park, G.-H., Paterson, K., Pierrot, D., Ríos, A. F., Sabine, C. L., Saito, S., Salisbury, J., Sarma, V. V. S. S., Schlitzer, R., Sieger, R., Skjelvan, I., Steinhoff, T., Sullivan, K. F., Sun, H., Sutton, A. J., Suzuki, T., Sweeney, C., Takahashi, T., Tjiputra, J., Tsurushima, N., van Heuven, S. M. A. C., Vandemark, D., Vlahos, P., Wallace, D. W. R., Wanninkhof, R., and Watson, A. J.: An update to the Surface Ocean CO_2 Atlas (SOCAT version 2), Earth Syst. Sci. Data, 6, 69–90, 2014.

Berti, S. and Lapeyre, G.: Lagrangian reconstructions of temperature and velocity in a model of surface ocean turbulence, Ocean Modelling, 76, 59–71, 2014.

Bouchet, F. and Venaille, A.: Statistical mechanics of two-dimensional and geophysical flows, Physics Reports, 515, 227–295, 2012.

Delcroix, T., Alory, G., Cravatte, S., Correge, T., and McPhaden, M.: A gridded sea surface salinity dataset for the tropical Pacific with sample applications (1950–2008), Deep-Sea Research I, 58(1), 38–48, 2011.

Dickey, T.: Emerging ocean observations for interdisciplinary data assimilation systems, J. Marine Syst., 40-41, 5–48, 2003.

Donlon, C. J., Martin, M., Stark, J., Roberts-Jones, J., Fiedler, E., and Wimmer, W.: The Operational Sea Surface Temperature and Sea Ice Analysis (OSTIA) system, Remote Sensing of Environment, 116, 140–158, 2012.

Franco, A. C., Hernández-Ayón, J. M., Beier, E., Garçon, V., Maske, H., Paulmier, A., Färber-Lorda, J., Castro, R., , and Sosa-Ávalos, R.: Air-sea CO_2 fluxes above the stratified oxygen minimum zone in the coastal region off Mexico, J. Geophys. Res. Oceans, 119, 2014.

Frisch, U.: Turbulence: The Legacy of A.N. Kolgomorov, Cambrige University Press, 1995.

Garbe, C. and Vihharev, J.: Modeling of atmospheric transport of chemical species in the Polar regions, in: IEEE International Geoscience and Remote Sensing Symposium, IEEE, Munich, Germany, 6047–6050, 22–27 July, 2012.

Garbe, C., Handler, R. A., and Jahne, B.: Transport at the Air–Sea Interface – Measurements, Models and Parameterizations, Springer-Verlag, Berlin, ISBN: 978-3-540-36904-2, 2007.

Garbe, C., Rutgersson, A., Boutin, J., Delille, B., Fairall, C., Gruber, N., Hare, J., Ho, D., Johnson, M., de Leeuw, G., Nightingale, P., Pettersson, H., Piskozub, J., Sahlee, E., Tsai, W., Ward, B., Woolf, D., and Zappa, C.: Transfer across the air–sea interface, in: Ocean–Atmosphere Interactions of Gases and Particles, edited by: Liss, P. and Johnson, M., Springer-Verlag, Norwich, UK, 55–112, 2014.

GLOBALVIEW: Cooperative Global Atmospheric Data Integration Project. 2013, updated annually. Multi-laboratory compilation of synchronized and gap-filled atmospheric carbon dioxide records for the period 1979-2012. Compiled by NOAA Global Monitoring Division: Boulder, Colorado, U.S.A. Data product accessed at http://dx.doi.org/10.3334/OBSPACK/1002, 2013.

González-Dávila, M., Santana-Casano, J., and Ucha, I.: Seasonal variability of fCO_2 in the Angola-Benguela region, Progress in Oceanography, 83(1-4), 124–133, 2009.

Gruber, N., Gloor, M., Fletcher, S., Doney, S., Dutkiewicz, S., and co authors: Oceanic sources, sinks and transport of atmospheric CO_2, Global Biogeochem. Cycles, 23, GB1005, 2009.

Gutknecht, E., Dadou, I., Vu, B. L., , Cambon, G., Sudre, J., Garçon, V., Machu, E., Rixen, T., Kock, A., Flohr, A., Paulmier, A., and Lavik, G.: Coupled physical/biogeochemical modeling including O_2-dependent processes in the Eastern Boundary Upwelling Systems: application in the Benguela, Biogeosciences, 10, 3559–3591, 2013.

Hales, B., Takahashi, T., and Bandstra, L.: Atmospheric CO_2 uptake by a coastal upwelling system, Global Biogeochem. Cycles, 19, GB1009, 2005.

IOCCP: Surface Ocean CO2 Variability and Vulnerabilities Workshop, Rep. 7, U.N. Educ., Sci. and Cult. Organ., Paris, 5, 2007.

Klein, P. and Lapeyre, G.: The oceanic Vertical Pump Induced by Mesoscale and Submesoscale Turbulence, Annu. Rev. Mar. Sci., 1, 351–75, 2009.

Landschützer, P., Gruber, N., Bakker, D., and Schuster, U.: Recent variability of the global ocean carbon sink, Global Biogeochem. Cycles, 28(9), 927–949, 2014.

Mahadevan, A., Lévy, M., and Mémery, L.: Mesoscale variability of sea surface pCO_2: What does it respond to?, Global Biogeochemical Cycles, 18, GB1017, 2004.

Maji, S. K. and Yahia, H. M.: Edges, transitions and criticality, Pattern Recognition, 47, 2104–2115, 2014.

Maritorena, S. and Siegel, D. A.: Consistent merging of satellite ocean color data sets using a bio-optical model, Remote Sensing of Environment, 94, 429–440, 2005.

Monteiro, P.: Eastern boundary currents: The Benguela Current System, in: Carbon and Nutrient Fluxes in Continental Margins: A Global Synthesis, Chap. 2, edited by Liu, K., Atkinson, L., Quiñones, R., and Talaue-McManus, L., Springer, Berlin, 2010.

Montes, I., Dewitte, B., Gutknecht, E., Paulmier, A., Dadou, I., Oschlies, A., and Garçon, V.: High-resolution modeling of the Eastern Tropical Pacific Oxygen Minimum Zone: Sensitivity to the tropical oceanic circulation, Journal of Geophysical Research: Oceans, p. accepted, 2014.

Paulmier, A., Ruiz-Pino, D., and Garçon, V.: The Oxygen Minimum Zone (OMZ) off Chile as intense source of CO_2 and N_2O, Continental Shelf Research, 28, 2746–2756, 2008.

Paulmier, A., Ruiz-Pino, D., and Garçon, V.: CO_2 maximum in the Oxygen Minimum Zone (OMZ), Biogeosciences, 8, 1–14, 2011.

Peters, W., Jacobson, A., C. Sweeney, A. A., Conway, T., Masarie, K., J.B. Miller, a. L. B., Petron, G., Hirsch, A., Worthy, D., van der Werf, G., Randerson, J., Wennberg, P., Krol, M., and Tans, P.: An atmospheric perspective on North American carbon dioxide exchange : CarbonTracker, Proceedings of the National Academy of Sciences of the USA, 104(48), 18 925–18 930, 2007.

Pfeil, B., Olsen, A., Bakker, D. C. E., Hankin, S., Koyuk, H., Kozyr, A., Malczyk, J., Manke, A., Metzl, N., Sabine, C. L., Akl, J., Alin, S. R., Bates, N., Bellerby, R. G. J., Borges, A., Boutin, J., Brown, P. J., Cai, W.-J., Chavez, F. P., Chen, A., Cosca, C., Fassbender, A. J., Feely, R. A., González-Dávila, M., Goyet, C., Hales, B., Hardman-Mountford, N., Heinze, C., Hood, M., Hoppema, M., Hunt, C. W., Hydes, D., Ishii, M., Johannessen, T., Jones, S. D., Key, R. M., Körtzinger, A., Landschützer, P., Lauvset, S. K., Lefèvre, N., Lenton, A., Lourantou, A., Merlivat, L., Midorikawa, T., Mintrop, L., Miyazaki, C., Murata, A., Nakadate, A., Nakano, Y., Nakaoka, S., Nojiri, Y.,

Omar, A. M., Padin, X. A., Park, G.-H., Paterson, K., Perez, F. F., Pierrot, D., Poisson, A., Ríos, A. F., Santana-Casiano, J. M., Salisbury, J., Sarma, V. V. S. S., Schlitzer, R., Schneider, B., Schuster, U., Sieger, R., Skjelvan, I., Steinhoff, T., Suzuki, T., Takahashi, T., Tedesco, K., Telszewski, M., Thomas, H., Tilbrook, B., Tjiputra, J., Vandemark, D., Veness, T., Wanninkhof, R., Watson, A. J., Weiss, R., Wong, C. S., and Yoshikawa-Inoue, H.: A uniform, quality controlled Surface Ocean CO_2 Atlas (SOCAT), Earth Syst. Sci. Data, 5, 125–143, 2013.

Pont, O., Turiel, A., and J., P.-V. C.: On optimal wavelet bases for the realization of microcanonical cascade processes, Int. J. Wavelets Multiresolut Inf. Process., 9(1), 35–61, 2011a.

Pont, O., Turiel, A., and Yahia, H.: An optimized algorithm for the evaluation of local singularity exponents in digital signals., vol. LNCS 6636 of *14th International Workshop on Combinatorial Image Analysis (IWCIA 2011)*, Springer-Verlag, Madrid, 2011b.

Pottier, C., Turiel, A., and Garçon, V.: Inferring mising data in satellite chlorophyll maps using turbulent cascading, Remote Sensing of Environment, 112, 4242–4260, 2008.

Rind, D. *et al.*.: Complexity and climate, Science, 284, 1999.

Rödenbeck, C., Bakker, D. C. E., Metzl, N., Olsen, A., Sabine, C., Cassar, N., Reum, F., Keeling, R. F., and Heimann, M.: Interannual sea–air CO_2 flux variability from an observation-driven ocean mixed-layer scheme, Biogeosciences, 11, 4599–4613, 2014.

Sabine, C. L., Hankin, S., Koyuk, H., Bakker, D. C. E., Pfeil, B., Olsen, A., Metzl, N., Kozyr, A., Fassbender, A., Manke, A., Malczyk, J., Akl, J., Alin, S. R., Bellerby, R. G. J., Borges, A., Boutin, J., Brown, P. J., Cai, W.-J., Chavez, F. P., Chen, A., Cosca, C., Feely, R. A., González-Dávila, M., Goyet, C., Hardman-Mountford, N., Heinze, C., Hoppema, M., Hunt, C. W., Hydes, D., Ishii, M., Johannessen, T., Key, R. M., Körtzinger, A., Landschützer, P., Lauvset, S. K., Lefèvre, N., Lenton, A., Lourantou, A., Merlivat, L., Midorikawa, T., Mintrop, L., Miyazaki, C., Murata, A., Nakadate, A., Nakano, Y., Nakaoka, S., Nojiri, Y., Omar, A. M., Padin, X. A., Park, G.-H., Paterson, K., Perez, F. F., Pierrot, D., Poisson, A., Ríos, A. F., Salisbury, J., Santana-Casiano, J. M., Sarma, V. V. S. S., Schlitzer, R., Schneider, B., Schuster, U., Sieger, R., Skjelvan, I., Steinhoff, T., Suzuki, T., Takahashi, T., Tedesco, K., Telszewski, M., Thomas, H., Tilbrook, B., Vandemark, D., Veness, T., Watson, A. J., Weiss, R., Wong, C. S., and Yoshikawa-Inoue, H.: Surface Ocean CO_2 Atlas (SOCAT) gridded data products, Earth Syst. Sci. Data, 5, 145–153, 2013.

Santana-Casiano, J., González-Dávila, M., and Ucha, I.: Carbon dioxide fluxes in the Benguela upwelling system during winter and spring: A comparison between 2005 and 2006, Deep Sea Research Part II, 56(8-10), 533–541, 2009.

Savtchenko, A., Ouzounov, D., Ahmad, S., Acker, J., Leptoukh, G., Koziana, J., and Nickless, D.: Terra and Aqua MODIS products available from NASA GES DAAC, Advances in Space Research, 34, 710–714, 2004.

Sudre, J., Yahia, H., Pont, O., and Garçon, V.: Ocean turbulent dynamics at super resolution from optimal multiresolution analysis and multiplicative cascade, in revision at IEEE TGRS, 2015.

Sweeney, C., Gloor, E., Jacobson, A., Key, R., McKinley, G., Sarmiento, J., and Wanninkhof, R.: Constraining global air-sea gas exchange for CO_2 with recent bomb 14C measurements, Global Biogeochemical Cycles, 21, GB2015, 2007.

Takahashi, T., Sutherland, S. C., Sweeney, C., Poisson, A., Metzl, N., Tilbrook, B., Bates, N., Wanninkhof, R., Feely, R., Sabine, C., Olafsson, J., and Nojiri, Y.: Global sea-air CO_2 flux based on climatological surface ocean pCO_2, and seasonal biological and temperature effects, Deep-Sea Research II, 49, 1601–1622, 2002.

Takahashi, T., Sutherland, S. C., Sweeney, C., Feely, R. A., Chipman, D. W., Hales, B., Friederich, G., Chavez, F., Sabine, C., Watson, A., Bakker, D. C. E., Schuster, U., Metzl, N., Yoshikawa-Inoue, H., Ishii, M., Midorikawa, T., Nojiri, Y., Kortzinger, A., Steinhoff, T., Hoppema, M., Olaffson, J., Anarson, T. S., Tilbrook, B., Johannessen, T., Olsen, A., Bellerby, R., Wong, C. S., Delille, B., Bates, N. R., , and de Baar, H. J. W.: Climatological mean and decadal change in surface ocean pCO_2, and net sea-air CO_2 flux over the global oceans, Deep-Sea Research II, 56, 554–577, 2009.

Telszewski, M., Chazottes, A., Schuster, U., Watson, A. J., Moulin, C., Bakker, D., M. González-Dávila and, T. J., Körtzinger, A., Lüger, H., Olsen, A., Omar, A., Padin, X. A., Ríos, A., Steinhoff, T., Santana-Casiano, M., Wallace, D. W. R., and Wanninkhof, R.: Estimating the monthly pCO_2 distribution in the North Atlantic using a self-organizing neural network, Biogeosciences Discuss., 6, 3373–3414, 2009.

Turiel, A., Isern-Fontanet, J., García-Ladona, E., and Font, J.: Multifractal Method for the Instantaneous Evaluation of the Stream Function in Geophysical Flows, Phys. Rev. Lett., 95, 104 502, 2005.

Turiel, A., Yahia, H., and Pérez-Vicente, C.: Microcanonical multifractal formalism-a geometrical approach to multifractal systems: PartI. Singularity analysis., J. Phys. A: Math. Theor., 41, 2008.

Valsala, V. and Maksyutov, S.: Simulation and assimilation of global ocean pCO_2 and air–sea CO_2 fluxes using ship observations of surface ocean pCO_2 in a simplified biogeochemical offline model, TellusB, 62B, 821–840, 2010.

Waldron, H. N., Monteiro, P. M. S., and Swart, N. C.: Carbon export and sequestration in the southern Benguela upwelling system: lower and upper estimates, Ocean Sci., 5, 711–718, 2009.

Weiss, R.: Carbon doxide in water and sewater: the solubility of a non-ideal gas, Marine Chemistry, 2, 203–215, 1974.

Yahia, H., Sudre, J., Pottier, C., and Garçon, V.: Motion analysis in oceanographic satellite images using multiscale methods and the energy cascade, Pattern Recognition, 43(10), 3591–3604, 2010.